UCRL-JC-117056
PREPRINT
CONF-941101--15

Stimulated BrillouinBackscatter of a Short-Pulse Laser

D. E. Hinkel
E. A. Williams
R. L. Berger

This paper was prepared for submittal to the
36th Annual Meeting of the APS Division of Plasma Physics
Minneapolis, MN
November 7-11, 1994

November 3, 1994

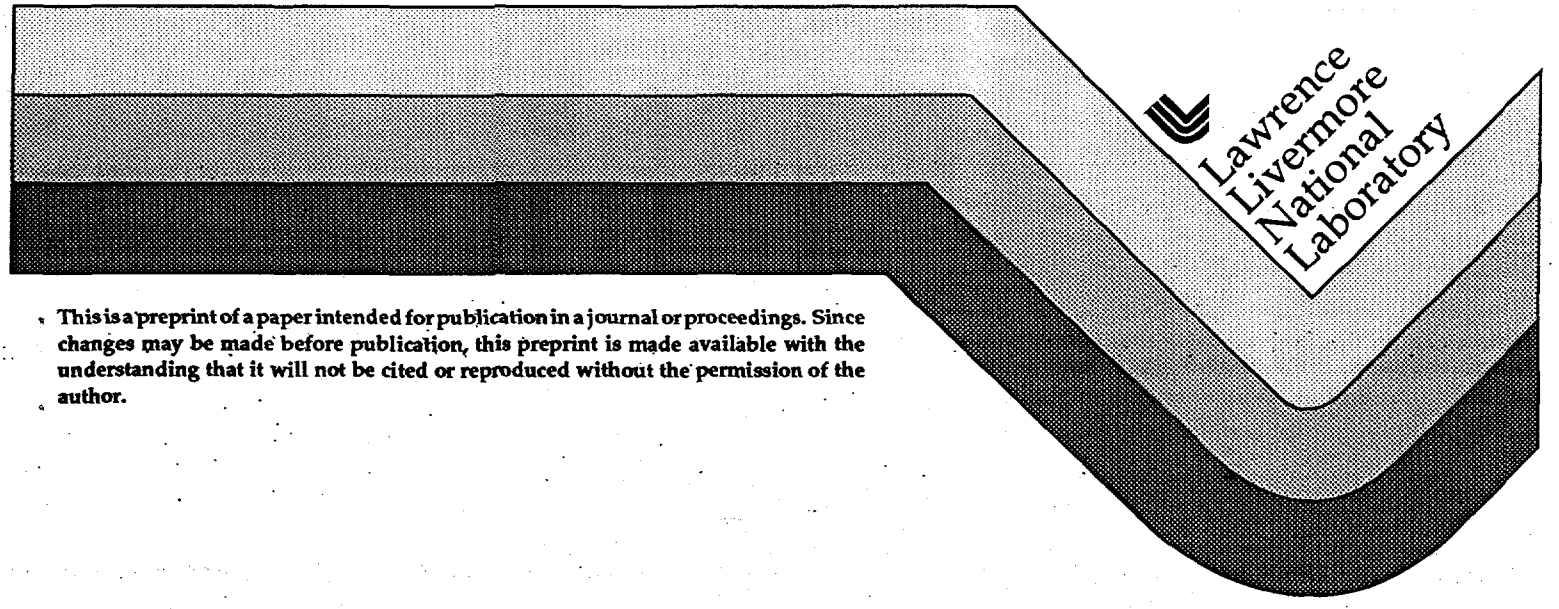

Stimulated Brillouin backscatter of a short-pulse laser

D. E. Hinkel, E. A. Williams, and R. L. Berger

Lawrence Livermore National Laboratory

P.O. Box 808, Livermore, CA 94550

(October 26, 1994)

Abstract

Stimulated Brillouin backscattering (SBBS) from a short-pulse laser, where the pulse length is short compared to the plasma length, is found to be qualitatively different than in the long pulse regime, where the pulse length is long compared to the plasma length. We find that after an initial transient of order the laser pulse length transit time, the instability reaches a steady state in the variables $x' = x - V_g t$, $t' = t$, where V_g is the pulse group velocity. In contrast, SBSS in a long pulse can be absolutely unstable and grows indefinitely, or until nonlinearities intervene. We find that the motion of the laser pulse induces Doppler related effects that substantially modify the backscattered spectrum at higher intensities, where the instability is strongly coupled (i.e., has a growth rate large compared to the ion acoustic frequency).

52.35Mw, 52.35Nx, 52.40Db, 52.40Nk

I. INTRODUCTION

Stimulated Brillouin backscatter (SBBS) is an instability which affects the coupling efficiency of the laser to plasma in laser-plasma interactions. In SBBS, a light wave incident on plasma scatters off ion acoustic density fluctuations. The scattered and incident light waves ponderomotively enhance the ion acoustic density fluctuations, which then cause further scattering.

There are many one-dimensional analyses of this parametric instability where the plasma is infinite in extent [1] - [5], as well as when the plasma is modelled as a finite slab [6] - [8]. For these cases, the pulse length is large compared to the plasma length and to the Rayleigh length, which is the distance measured from the focal plane over which the laser intensity decreases by a factor of two. Also of interest is SBBS in the presence of a short-pulse laser, [9], [10], where the plasma length is large compared to the pulse length.

Short-pulse lasers [11] have a wide range of applications. In x-ray lasing [12], a high-intensity, short-pulse laser is used to optically field ionize plasma, after which recombination occurs. Harmonic generation [13,14] takes place when a high-intensity, short-pulse laser propagates through plasma. Creation of plasma by gas ionization with an intense, short-pulse laser [15], which causes frequency upshifting of the laser pulse, yields knowledge of initial plasma conditions such as temperature, density and charge state. Short-pulse lasers may also be potentially useful as a time and space resolved diagnostic for inertial confinement fusion (ICF) experiments. If the amount of energy backscattered by parametric instabilities such as SBBS is significant, then the laser energy available to drive the above-mentioned processes is altered. A detailed understanding of SBBS is therefore useful in interpreting experimental results and in suppressing its occurrence in short-pulse laser applications.

When the pulse length is long compared to the plasma length, SBBS can be absolutely unstable provided the spatial growth rate exceeds the mean spatial damping rate. In contrast, when the plasma length is long compared to the pulse length, SBBS can never be absolutely unstable, even in the absence of damping. Rather, the instability grows only

where the pump pulse is present; once the pulse has passed by, the instability has no more temporal growth. In fact, even in terms of the variables $x' = x - V_g t$, $t' = t$, where V_g is the pulse group velocity, SBBS is not absolutely unstable, because in this frame the scattered light wave and ion acoustic waves propagate in the same direction, making the instability convective. Thus, the temporal evolution of SBBS in a short pulse is qualitatively different than that of SBBS in the more familiar situation of a plasma where the pulse length is long compared to the plasma length.

In this paper we examine and analyze the spatio-temporal evolution of SBBS in a plasma whose length is long compared to that of the pulse. We perform this analysis in both the weak and strong coupling limits, where the growth rate is small or large compared to the ion acoustic frequency, respectively.

We show that there are three temporal regimes for short pulse SBBS. In the early time regime, $t < \tau/2$, where τ is the amount of time it takes the pump pulse to traverse a fixed spatial location inside the plasma, there is temporal growth of the instability. In the weak coupling limit the growth rate is $\Gamma = \gamma_0$, where γ_0 is the infinite medium weak coupling growth rate. When the instability is strongly coupled, the initial growth rate is approximately $\Gamma \sim (2\gamma_0^2\omega_a)^{1/3}$, where ω_a is the ion acoustic frequency.

During the intermediate time regime, $\tau/2 < t < \tau$, the growth rate drops to zero in both the weak and strong coupling limits. For this time regime, we have derived an exact expression for the scattered light wave amplitude in the weak coupling limit.

Finally, in the late time regime, $t \geq \tau$, the instability reaches a steady state in terms of the variables $x' = x - V_g t$, $t' = t$, and the wave amplitudes exponentiate from the front to the back of the pulse. In the weak coupling limit the spatial amplification rate is given by the expression $\kappa = \gamma_0/(2^{1/2}c)$. This is the usual forward scatter weak coupling spatial amplification rate $\gamma_0/(V_1 V_2)^{1/2}$, with $V_1 = -2c$ and $V_2 = -c$ in the pulse frame.] In the strong coupling limit, the spatial gain is approximately $\kappa \sim (\gamma_0^2\omega_a)^{1/3}/c$. We have performed numerical investigations of both the weak and strong coupling limits, encompassing all three time regimes, and find good agreement between our numerical results and our analytic

predictions.

In arriving at these conclusions we have made the following assumptions. We have treated the plasma as uniform, and have neglected pump depletion. Pump depletion acts to limit scatter, and thus should be incorporated when the scattered light wave grows up to roughly the level of the pump wave. In treating the plasma as uniform we have assumed the pulse length is short compared to the velocity, temperature and density scale lengths. We have also neglected the effects of damping, which is valid provided $\gamma_0 \gg \nu$, where ν is the ion acoustic wave damping rate. This is the usual requirement, $\gamma_0 \gg \nu(V_1/V_2)^{1/2}$, but applied in the pulse frame, so that $V_1 = -2c$ is the speed of the scattered light wave, and $V_2 = -c$ is the ion acoustic wave speed. In "long" pulse SBBS, where the pulse length is long compared to the plasma length, $V_1 \approx c$ and $V_2 = C_s \ll c$ [C_s is the ion acoustic wave speed], which yields a more stringent condition for neglecting damping, namely $\gamma_0 \gg \nu(c/C_s)^{1/2}$.

Finally, we have also chosen to treat the plasma as underdense, where $n \ll n_c$, which is a regime of relevance to current short pulse experiments [16]. In principle we are able to treat (both numerically and theoretically) the more general case of a short laser pulse propagating through plasma of arbitrary sub-critical density.

In a scattering experiment, the instability would grow up from a spectrum of density fluctuations as is modelled by Ref. [9]. Here we have chosen to model the short pulse problem with a simple set of boundary and initial conditions on the scattered light wave. We are justified in doing so, as we find that within a relatively short amount of time, e.g., $t = \tau$, the system has entered a steady state where the gain factor is independent of the initial conditions of the problem. Finally, in calculating the low frequency response to a short pulse laser we anticipate that the frequency spectrum will be broad, as the amount of time that the density fluctuations are influenced by the laser is typically less than a few ion acoustic wave periods.

This paper is organized as follows. In Sec. II, we introduce the theoretical model in the lab variables (x, t) and perform a change of variables, $x' = x - V_g t$, $t' = t$, which we find makes analysis more straightforward. In Sec. III we determine exact solutions for the wave

amplitudes in the weak coupling limit, and approximate solutions for the wave amplitudes in the strong coupling limit. We also analyze the power spectrum and dispersion relation in the steady state regime in both the weak and strong coupling limits. In Sec. IV, we perform a numerical analysis of short pulse SBBS, and verify our analytic estimates. The results are summarized in Sec. V.

II. THEORETICAL MODEL

In stimulated Brillouin backscatter a light wave incident on plasma scatters off density fluctuations. The incident and scattered light waves beat with one another and ponderomotively drive density fluctuations, which then cause further scattering. This process can be described by the following set of envelope equations for the instability [8]:

$$\left[\frac{\partial}{\partial t} - V_g\frac{\partial}{\partial x} + \frac{ic^2}{2\omega_1}\frac{\partial^2}{\partial x^2}\right] a_1 \;=\; \gamma_0 a_2 \quad , \tag{1a}$$

$$\left[\frac{\partial^2}{\partial t^2} - 2i\omega_a\frac{\partial}{\partial t} - 2i\omega_a C_s\frac{\partial}{\partial x} - C_s^2\frac{\partial^2}{\partial x^2}\right] a_2 = -2i\omega_a\gamma_0\left[1 - \frac{i}{k_0}\frac{\partial}{\partial x} - \frac{1}{4k_0^2}\frac{\partial^2}{\partial x^2}\right] a_1 \quad , \tag{1b}$$

where $V_g \equiv c^2k_1/\omega_1$ is the scattered light wave group velocity, ω_0 (ω_1) is the incident (scattered) light wave frequency, $\omega_a \equiv 2k_0C_s$ is the ion acoustic wave frequency, k_0 (k_1) is the incident (scattered) light wavenumber, $k_a \equiv 2k_0$ is the ion acoustic wavenumber for backscatter, and $C_s \equiv [ZT_e/M]^{1/2}$ is the sound speed. Here, Z is the ionic charge state, T_e is the electron temperature, and M is the ionic mass. The coupling parameter is $\gamma_0 \equiv k_0v_0\omega_{pi}/(\omega_0\omega_a)^{1/2}$, where $\omega_{pi} \equiv (4\pi Z^2n_ie^2/M)^{1/2}$ is the ion plasma frequency, with n_i the ionic plasma density and $-e$ the electronic charge. The oscillatory velocity of an electron in an electric field is $v_0 \equiv eb_0/(mc)$, where b_0 is the envelope of the incident wave vector potential $\{A_0 = b_0(x,t)\exp[i(k_0x - \omega_0t)] - \text{c.c.}\}$ and m is the electron mass. Analogously, the variable we use to describe the scattered light wave is $a_1 \equiv eb_1^*/(mcC_s)$, with

$A_1 = b_1(x,t)\exp[i(k_0x - \omega_0t)] + \text{c.c.}$ Also, the ion acoustic wave is mathematically typified by the expression $a_2 \equiv [i\omega_{pe}^2/(2\omega_{pi})][e^{-i\arg(a_0)}/(\omega_0\omega_a)^{1/2}]\delta n/n_e$, where $\omega_{pe} \equiv (4\pi n_e e^2/m)^{1/2}$ is the electron plasma frequency, n_e is the electron plasma density, and δn is the envelope of the density fluctuation, $n = \delta n(x,t)\exp[i(k_ax - \omega_at)]$. In deriving these equations, we have neglected the Stokes' terms, namely $\exp\{i[3k_0x - (\omega_0 + \omega_a)t]\}$, which has frequency and wavenumber far from that of the scattered light wave, $\exp[i(k_1x - \omega_1t)]$, as well as $\exp[-i(2\omega_0 - \omega_a)t]$, which has wavenumber and frequency far from that of the density fluctuation, $\exp[i(2k_0x - i\omega_at)]$. Finally, we have also neglected the ∂_t^2 term in the light wave equation, which is of importance only early in time, i.e., for times $t \ll \omega_0^{-1} \ll L/c$, where L is the pulse length.

It is convenient to make a change of variables when analyzing short pulse problems [17], so that the pulse boundary conditions are fixed. In terms of these new variables, where $x' = x - V_gt \approx x - ct$ and $t' = t$, the set of equations (1) takes the form

$$\left[\frac{\partial}{\partial t'} - 2c\frac{\partial}{\partial x'} + \frac{ic^2}{2\omega_1}\frac{\partial^2}{\partial x'^2}\right] a_1 = \gamma_0 a_2 \quad , \tag{2a}$$

$$\left[\frac{\partial^2}{\partial t'^2} - 2i\omega_a\frac{\partial}{\partial t'} - 2c\frac{\partial}{\partial x'}\frac{\partial}{\partial t'} - 2i\omega_a c\frac{\partial}{\partial x'} + c^2\frac{\partial^2}{\partial x'^2}\right] a_2 =$$
$$-2i\omega_a\gamma_0\left[1 - \frac{i}{k_0}\frac{\partial}{\partial x'} - \frac{1}{4k_0^2}\frac{\partial^2}{\partial x'^2}\right] a_1. \tag{2b}$$

For simplicity we consider an underdense plasma, so that we can approximate the pulse group velocity $V_g = c\sqrt{1 - n/n_c} \approx c$.

As shown in Fig. 1, in this reference frame, the pulse is stationary and the scattered light wave grows up from noise at the head of the pulse (at $x' = L$), is amplified as it moves backward across the pulse (toward $x' = 0$), and then free streams toward the detector (located at $x' < 0$).

In the following sections this set of equations (2) will be analyzed in the weak coupling limit, where the growth rate is small compared to the ion acoustic frequency, $|\partial_t a_2| \ll |\omega_a a_2|$,

and the spatial rate of change of the envelopes is small compared to the vacuum wavenumber, $|\partial_x a_{1,2}| \ll |k_0 a_{1,2}|$, as well as in the strong coupling limit, where $|\partial_t a_2| \geq |\omega_a a_2|$ but $|\partial_x a_{1,2}| \ll |k_0 a_{1,2}|$.

III. ANALYSIS

We have determined [8] that the SBBS instability in a system where the pulse length and the Rayleigh length exceed the plasma length exhibits generic behavior which is dependent upon the whether the modes are weakly or strongly coupled. Such a model is also suitable for the short pulse SBBS problem, where the pulse length is short compared to the Rayleigh length and the plasma length. In this section we analyze short pulse SBBS in first the weak coupling limit, where we have found an exact solution, and also in the strong coupling limit where we have determined approximate solutions based upon the amount of time the instability has had to evolve.

The short pulse SBBS scenario depicted in Fig. 1 applies equally well in both the weak and strong coupling limits. In Region I of Fig. 1, in front of the pulse, there exists thermal fluctuations in the plasma which the pulse has not yet encountered. In Region II of Fig. 1, inside the pulse, the scattered light wave is amplified as it convects across the pulse. In Region III of Fig. 1, behind the pulse, the scattered light wave has left the pulse and free streams toward the detector.

For the sake of clarity we have chosen to drive just the resonant mode of the problem, which, after a few e-foldings will dominate the spectrum. To make contact with previous analytic work [8,18] the following set of initial and boundary conditions is used:

$$a_1(x', t' = 0) = \bar{a} \quad , \tag{3a}$$

$$a_2(x', t' = 0) = 0 \quad , \tag{3b}$$

$$a_1(x' > L, t') = \bar{a}\, H(t') \quad , \tag{3c}$$

$$a_2(x' > L, t') = 0 \quad , \tag{3d}$$

where $H(t')$ is the usual Heaviside function, $H = 0$, $t' < 0$, $H = 1$, $t' > 0$.

Rather than modelling the thermal fluctuations in the plasma, as in Ref. [9], we have chosen to drive the problem from a constant level of scattered light wave within the system. At time $t = 0$, this level of constant scattered light wave exists everywhere in the plasma. This set of initial and boundary conditions will be used in both the weak and strong coupling limits.

A. Causal Analysis

Before analyzing SBBS in either the weakly or strongly coupled limit, it is instructive to examine a causality diagram, such as that of Fig. 2, which clearly depicts the spatio-temporal behavior of the instability. In Fig. 2, the line $t' = (L - x')/(2c)$ denotes a scattered light wave generated at $x' = L$ travelling to the left, which reaches $x' = 0$ at time $t' = L/(2c)$. All points below this line reside in the early time regime. The line $t' = (L - x')/c$ depicts an ion acoustic wave produced at $x' = L$ which encounters the lefthand boundary at time $t' = L/c$. All points above this line lie in the late time regime. For times $(L - x')/(2c) \leq t' \leq (L - x')/c$ the instability is in the intermediate time regime, where the scattered light wave has had time to cross the laser pulse but the ion acoustic wave has not.

Consider point a of Fig. 2, which resides in the early time regime. Its causal region is enclosed by the dashed lines - - -. Point a is influenced by the initial conditions and not by the boundary conditions. Since the initial conditions are independent of the spatial variable the instability can only have a temporal dependence in this regime.

A point such as b in Fig. 2 resides in the late time regime. Its causal region of influence, denoted by - - - , is affected by the boundary condition at $x' = L$, which is time independent. Thus in this temporal regime the instability can only have a spatial dependence.

The causal region of influence for point c, located in the intermediate time regime, is enclosed by the dashed lines, - - - - . From Fig. 2, however, it is evident that when the instability is in the intermediate time regime, it is affected by the boundary conditions at $x' = L$ as well as by the initial conditions, thereby leading to both spatial and temporal dependence.

B. Weak Coupling Limit

In this sub-section we invoke the causal analysis of the previous sub-section to obtain analytic expressions for the scattered light wave amplitude in the early and the late time regimes. {Once the scattered light wave amplitude is determined, the ion acoustic wave amplitude is also determined, as $a_2 = \gamma_0^{-1}[\partial_{t'} - 2c\partial_{x'} + ic^2/(2\omega_1)\partial x'^2]a_1$.}

We have also derived an exact solution for the scattered light wave amplitude. From the exact solution, which entails infinite sums over modified Bessel functions, we extract the early and late time regime behavior of the instability and find it to be identical to the behavior determined by solving the approximate differential equations appropriate to the early and late time regimes.

In the lab frame the scattered light wave and density fluctuations are weakly coupled when $|\partial_t a_2| \ll |\omega_a a_2|$ and $|\partial_x a_{1,2}| \ll |k_0 a_{1,2}|$. In terms of the variables $x' = x - ct$, $t' = t$, this weak coupling condition takes the form

$$\left|\left(\frac{\partial}{\partial t'} - c\frac{\partial}{\partial x'}\right) a_2\right| \ll |\omega_a a_2| \quad ; \tag{4a}$$

$$\frac{\partial}{\partial x'} a_{1,2} \ll |k_0 a_{1,2}| \quad . \tag{4b}$$

When this limit is applied to the set of equations (2) the weakly coupled set of equations in the pulse frame are found to be of the form

$$\left[\frac{\partial}{\partial t'} - 2c\frac{\partial}{\partial x'}\right] a_1 = \gamma_0 a_2 \quad . \tag{5a}$$

$$\left[\frac{\partial}{\partial t'} - c\frac{\partial}{\partial x'}\right] a_2 \;=\; \gamma_0 a_1 \quad . \tag{5b}$$

We can apply what we have learned about SBBS from a causal analysis to this set of equations to obtain the behavior of the instability in the early time regime, where $t' < (L - x')/(2c)$, and in the late time regime, where $t' > (L - x')/c$. In the early time regime, where the instability is affected by the spatially independent initial conditions, $|c\partial_{x'}| \ll |\partial_{t'}|$, and the set of equations (5) reduces to

$$\frac{\partial}{\partial t'} a_1 \;=\; \gamma_0 a_2 \quad , \tag{6a}$$

$$\frac{\partial}{\partial t'} a_2 \;=\; \gamma_0 a_1 \quad , \tag{6b}$$

or

$$\frac{\partial^2}{\partial t'^2} a_1 = \gamma_0^2 a_1 \quad . \tag{7}$$

Eq. (7) is readily solvable, subject to the initial condition as given by (3a), and we find

$$a_1[t' \leq (L - x')/(2c)] \;=\; \bar{a} H(t') \cosh(\gamma_0 t') \quad . \tag{8}$$

Analogously, in the late time regime, the causal analysis of the previous sub-section indicated that for times $t \geq (L - x')/c$, the instability has no temporal variation since the boundary conditions as given by (3) are temporally independent. For these times, $|\partial_{t'} \ll |c\partial_{x'}|$, and the set of equations (5) reduces to

$$2c^2 \frac{\partial^2}{\partial x'^2} a_1 \;=\; \gamma_0^2 a_1 \quad , \tag{9}$$

with solution

$$a_1[(L - x')/c \leq t'] \;=\; \bar{a} \cosh[\gamma_0 (x' - L)/(\sqrt{2}c)] \quad . \tag{10}$$

The early time and late time behavior can be extracted from the exact solution as well. The exact solution is determined by performing a Laplace transform in time, and solving

for $a_1(x',\omega')$ in the three different regions (c.f. Fig. 1), where ω' is the transform variable. The expressions for a_1 in the three different regions are matched at the pulse edges, and the inverse Laplace transform back to the temporal variable is performed. Such a procedure yields

$$
\begin{aligned}
a_1(x',t') \;=\; & \bar{a}H(t')H(x'-L) \\
& + \bar{a}\,[H(x') - H(x'-L)]\left[H(t')\cosh(\gamma_0 t')\right. \\
& + H\left(t' + \frac{x'-L}{2c}\right)\sum_{m=0}^{\infty}(2^m-1)\left(i\sqrt{\frac{\beta}{\alpha}}\right)^{2m} I_{2m}\left(-\frac{2i\gamma_0}{c}\sqrt{\alpha\beta}\right) \\
& \left. - H\left(t' - \frac{x'-L}{c}\right)\sum_{m=0}^{\infty}(2^m-1)\left(i\sqrt{\frac{\alpha}{2\beta}}\right)^{2m} I_{2m}\left(-\frac{2i\gamma_0}{c}\sqrt{\alpha\beta}\right)\right] \\
& + \bar{a}H(-x')\left[H(t') - H(t'+\frac{x'}{2c})\right] + \; a_1(x'=0,t'+\frac{x'}{2c})\; H(-x') \quad . \qquad \text{(11a)}
\end{aligned}
$$

$$
\alpha \;\equiv\; 2ct' + x' - L \quad , \qquad \text{(11b)}
$$

$$
\beta \;\equiv\; ct' + x' - L \quad . \qquad \text{(11c)}
$$

In front of the puise ($x' > L$), for all time, the scattered light wave has constant amplitude $\bar{a}$. Inside the pulse ($0 \le x' \le L$), the formal solution as given by (11a) contains the three generic temporal regimes discussed in the causal analysis. For times $0 \le t' \le (L-x')/(2c)$, i.e., before the scattered light wave has crossed the pulse, Eq. (11a) is of the form

$$
a_1(0 \le x' \le L, 0 \le t' \le \frac{L-x'}{2c}) \;=\; \bar{a}\,\cosh(\gamma_0 t') \quad , \qquad \text{(12)}
$$

which is precisely the early time solution (8) determined from the set of equations (6). When the early time solution is utilized in (4a), the weak coupling condition becomes $\gamma_0 \ll \omega_a$, which is the typical weak coupling condition for SBBS in a finite slab. [8]

For times $t' \ge (L-x')/c$, i.e., after the ion acoustic wave has transited the pulse (in the pulse frame), all of the terms of (11a) for $0 \le x' \le L$ are non-zero. It is straightforward to show [19] that the infinite sums collapse to cosh functions:

$$\cosh\left[\gamma_0 t'\right] - \cosh\left[\frac{\gamma_0}{\sqrt{2}c}(x' - L)\right]$$
$$= \sum_{m=0}^{\infty}(-1)^m \left[\left(\sqrt{\frac{\alpha}{\beta}}\right)^{2m} - \left(\sqrt{\frac{\alpha}{2\beta}}\right)^{2m}\right]$$
$$\times I_{2m}\left[-\frac{2i\gamma_0}{c}\sqrt{\alpha\beta}\right] \quad . \tag{13}$$

Thus in this time regime the scattered light wave is given by the expression

$$a_1\left(0 \le x' \le L, \frac{L - x'}{c} \le t'\right) = \bar{a}\cosh\left[\frac{\gamma_0}{\sqrt{2}c}(x' - L)\right], \tag{14}$$

which is the late time solution (10) as determined from (9). When the late time solution is utilized in (4a), the weak coupling condition becomes $\gamma_0 \ll \sqrt{2}\omega_a$. Thus, for all time the weak coupling condition, (4a), is consistent with the finite slab weak coupling condition, $\gamma_0 \ll \omega_a$.

Early in time, $[0 \le t' \le L/(2c)]$, then, the light wave has only temporal dependence inside the pulse, whereas late in time $[L/c \le t']$ there is only a spatial gain across the pulse. The growth rate, defined as $|\dot{a}_1(x', t')/a_1(x', t')|$, is roughly γ_0 early in time, and then drops to zero by time $t' = L/c$. This is clearly shown in Sec. IV where a numerical analysis of the short pulse problem is undertaken.

C. Strong Coupling Limit

In the lab frame the scattered light wave and density fluctuations are strongly coupled when $|\partial_t a_2| \ge |\omega_a a_2|$ but $|\partial_x a_{1,2}| \ll |k_0 a_{1,2}|$, i.e., the growth rate of the ion acoustic wave is of the order or larger than the acoustic frequency, but the spatial rate of change of either wave is small compared to the vacuum wavenumber. In terms of the variables $x' = x - ct$, $t' = t$, this strong coupling condition is

$$\left|\left(\frac{\partial}{\partial t'} - c\frac{\partial}{\partial x'}\right)a_2\right| \ge |\omega_a a_2| \quad , \tag{15a}$$

$$\frac{\partial}{\partial x'}a_{1,2} \ll k_0 a_2 \quad . \tag{15b}$$

Applying (15) to the set of equations (2) yields the strongly coupled set of equations in the pulse frame.

$$\left[\frac{\partial}{\partial t'} - 2c\frac{\partial}{\partial x'}\right] a_1 = \gamma_0 a_2 \quad ; \tag{16a}$$

$$\left[\frac{\partial^2}{\partial t'^2} - 2i\omega_a\frac{\partial}{\partial t'} - 2c\frac{\partial}{\partial x'}\frac{\partial}{\partial t'} + 2i\omega_a c\frac{\partial}{\partial x'} + c^2\frac{\partial^2}{\partial x'^2}\right] a_2 = -2i\omega_a\gamma_0 a_1 \quad . \tag{16b}$$

While we have been unsuccessful in determining an exact solution to the strongly coupled set of equations (16) we have been able to approximate the scattered light wave amplitude early in time $[0 \leq t' \leq L/(2c)]$, i.e., before the light wave has transited the pulse, and late in time $[L/c \leq t']$, after the ion acoustic wave has crossed the pulse. We have found that the temporal growth and spatial gain rates of the strongly coupled instability have the same qualitative features as when the instability is weakly coupled; however, quantitative differences in the growth and gain rates exist between the two coupling limits.

Early in time, before the scattered light wave has crossed the pulse, $0 \leq t' \leq L/(2c)$, neither wave knows about the pulse boundaries; moreover, since the initial conditions are spatially constant, there is no spatial variation in the pulse frame, or $\partial_{x'} a_{1,2} = 0$. Within this early time approximation the set of equations which describes the evolution of the strongly coupled instability collapses to

$$\left(\frac{d^3}{dt'^3} - 2i\omega_a\frac{d^2}{dt'^2} + 2i\omega_a\gamma_0^2\right) a_1 = 0 \quad . \tag{17}$$

When the ansatz $a_1 = \bar{a}\exp(-i\omega_a\delta t')$ is made, Eq. (17) takes the form

$$\delta^3 + 2\delta^2 + 2\gamma_0^2 = 0. \tag{18}$$

Late in time, after both waves have transited the pulse, i.e., for times $t' > L/c$, the problem is dominated by spatial variation, or $|c\partial_{x'}| \gg |\partial_{t'}|$. For these late times the set of equations describing the spatial evolution of the strongly coupled instability can be written as

$$\left(\frac{d^3}{dx'^3} + 2i\frac{\omega_a}{c}\frac{d^2}{dx'^2} - i\frac{\gamma_0^2\omega_a}{c^3}\right) a_1 = 0 \quad . \tag{19}$$

When the substitution $a_1 = \bar{a}\,\exp(i\omega_a\eta x'/c)$ is made in (19), there exists a cubic equation in η to solve:

$$\eta^3 + 2\eta^2 + \frac{\gamma_0^2 c^3}{\omega_a^2} = 0 \quad . \tag{20}$$

Both Eqs. (17) and (19) are of the form

$$y^3 + 2y^2 + \alpha(\gamma_0/\omega_a)^2 = 0 \quad , \tag{21}$$

where $\alpha = 2$ for the early time solution, and $\alpha = 1$ for the late time solution. A solution for y is determined by making a power series expansion in terms of the ratio of the acoustic frequency to the coupling parameter, ω_a/γ_0, where here, for the strongly coupled problem, $\gamma_0 \geq \omega_a$:

$$y \equiv b_1\left(\frac{\gamma_0}{\omega_a}\right)^{2/3} + b_2 + b_3\left(\frac{\gamma_0}{\omega_a}\right)^{-2/3} + b_4\left(\frac{\gamma_0}{\omega_a}\right)^{-4/3} + \ldots \tag{22}$$

Eq. (21) can be solved order by order in powers of ω_a/γ_0 using the series expansion (22), which yields

$$\begin{aligned} b_1 &= (-\alpha)^{1/3} \quad , \\ b_2 &= -\frac{2}{3} \quad , \\ b_3 &= \frac{4}{9\alpha}(-\alpha)^{2/3} \quad , \\ b_4 &= \frac{16}{81\alpha}(-\alpha)^{1/3} \quad . \end{aligned} \tag{23}$$

The cubic root of α is chosen to yield growth for the early time and late time solutions, i.e., $b_1 = 2^{1/3}e^{i\pi/3}$ for the early time solution, and $b_1 = e^{-i\pi/3}$ for the late time solution. We find that, early in time,

$$\begin{aligned} a_1 \sim \bar{a}\; H(t')\exp\Big[-i\omega_a t\Big(&2^{1/3}e^{i\pi/3}(\gamma_0/\omega_a)^{2/3} \\ &-\frac{2}{3} - \frac{2}{9}2^{2/3}e^{-i\pi/3}(\omega_a/\gamma_0)^{2/3} \\ &-\frac{8}{81}2^{1/3}e^{i\pi/3}(\omega_a/\gamma_0)^{4/3} + \ldots\Big)\Big] \end{aligned} \tag{24}$$

Analogously, late in time,

$$a_1 \sim \bar{a} \exp\left[i\frac{\omega_a x'}{c}\left(e^{-i\pi/3}(\gamma_0/\omega_a)^{2/3} - \frac{2}{3} + \frac{4}{9}e^{i\pi/3}(\omega_a/\gamma_0)^{2/3} + \frac{16}{81}(\omega_a/\gamma_0)^{4/3} + \ldots\right)\right] \quad . \tag{25}$$

Eqs. (24) and (25) bring forth the following features with respect to the behavior of the scattered light wave. In the early time regime, there is only temporal growth, as when the instablity is weakly coupled, but the rate of temporal growth is $\Gamma \equiv |\dot{a}_1/a_1| \sim 2^{1/3}(\gamma_0^2\omega_a)^{1/3}$ as compared with the weakly coupled temporal growth rate, $\Gamma \sim \gamma_0$. These early time temporal growth rates are identical to those in a finite plasma slab where the instability is driven from a spatially constant initial condition [8]. In the late time regime, there is only spatial gain, as in the weak coupling limit, but the rate of spatial change is $\kappa \equiv |a_1'/a_1| \sim (\gamma_0^2\omega_a)^{1/3}/c$, in contrast with the weakly coupled spatial rate of change, $\kappa \sim \gamma_0/(\sqrt{2}c)$.

A numerical solution is necessary to describe the instability in the strongly coupled limit during the intermediate time regime. However, from Fig. 2 it is evident that during the intermediate time regime the instability is affected by the boundary conditions at $x' = L$ as well as by the initial conditions, thereby leading to both spatial and temporal dependence.

D. Power Spectrum

Independent of the pump strength, the instability grows for a time $\tau = L/c$, after which there exists a spatial gain across the pulse. Typically, short-pulse experiments [16] collect signal for several pulse length transit times (τ), and thus the power spectrum is dominated by the steady state rather than by the initial transient growth. Were this not the case a more complicated model, taking into account the spatial profile of the plasma, would have been required.

To this end, we have analyzed the problem depicted in Fig. 3. In terms of the steady state variables, $x' = x - ct$, $t' = t$, in Region I, there is a noise level of scattered light

wave, given by $a_I = \bar{a}\ \exp[i(k'_{uc}x' - \Omega' t')]$. In front of the pulse the scattered light wave and the density fluctuations are uncoupled, and thus the scattered light wave obeys the dispersion relation $k'_{uc} = -\Omega'/(2c)$, where Ω' is real. Inside the pulse (Region II of Fig. 3) the scattered light wave is of the form $a_{II} = \bar{a}\ \exp[i(k'_{sc}x' - \Omega' t')]$, where Ω' is real and k'_{sc} obeys the strongly coupled dispersion relation,

$$\left(\overline{k}' - \overline{k}'_a\right)\left(\overline{k}' - \overline{k}'_b\right)\left(\overline{k}' - \overline{k}'_c\right)\left(\overline{k}' - \overline{k}'_d\right) + \frac{16\overline{\gamma}_0^2\epsilon^3}{\delta}\left(1 + \overline{k}' + \overline{k}'^2/4\right) = 0, \qquad (26)$$

with $\overline{k}' \equiv k'_{sc}/k_0$, $\overline{\gamma}_0 \equiv \gamma_0/\omega_a$, $\epsilon \equiv C_s/c$, $2\delta \equiv n/n_c$, and

$$\overline{k}'_a = -\epsilon\overline{\Omega}' \ , \qquad (27a)$$

$$\overline{k}'_b = -2\epsilon\left(1 - \epsilon\overline{\Omega}'\right)/\delta \ , \qquad (27b)$$

$$\overline{k}'_c = -2\epsilon(\overline{\Omega}' + 2)/(1 + \epsilon) \ , \qquad (27c)$$

$$\overline{k}'_d = -2\epsilon\overline{\Omega}'/(1 - \epsilon) \ . \qquad (27d)$$

Here, $\overline{\Omega}'$ denotes the frequency variable Ω' normalized to the ion acoustic frequency, ω_a. Moreover, $\overline{k}'_a$ represents the uncoupled scattered light wave, $\overline{k}'_b$ represents the uncoupled forward scattered light wave, $\overline{k}'_c$ represents an uncoupled ion acoustic wave (which would propagate in the direction opposite the pulse group velocity, or "backward" in the lab frame), and $\overline{k}'_d$ represents the other uncoupled ion acoustic wave (which would propagate in the same direction as the pulse in the lab frame, or "forward"). In deriving this dispersion relation we have retained all terms in the set of equations (2).

On the back side of the pulse (Region III), the scattered light wave is again uncoupled from the density fluctuations, and so is of the form $a_{III} \sim \bar{a}\ \exp[i(k'_{uc}x' - \Omega' t')]$, where Ω' is real and $k'_{uc} = -\Omega'/(2c)$. When the solutions in the three regions are matched at the boundaries $x' = 0$ and $x' = L$ we find that

$$a_1(x' \geq L) = \bar{a}\ \exp\{i[k'_{uc}(x' - L) - \Omega' t']\} \ , \qquad (28a)$$

$$a_1(0 \leq x' \leq L) = \bar{a}\ \exp\{i[k'_{sc}(x' - L) - \Omega' t']\} \ , \qquad (28b)$$

$$a_1(x' \leq 0) \;=\; \bar{a}\,\exp\{i\,[k'_{uc}x' - \Omega' t' - k'_{sc}L]\} \quad . \tag{28c}$$

In Region I, before the scattered light wave has travelled through the pulse, it has magnitude $\bar{a}$. In Region III, after the scattered light wave has transited the pulse, it has magnitude $\bar{a}\,\exp(G)$, where the spatial gain $G \equiv \mathrm{Im}(k'_{sc})L$. Thus, by determining the imaginary part of the strongly coupled wavenumber in the pulse frame we can construct the power spectrum, $P \equiv \exp(2G)$.

It is instructive to examine the evolution of the dispersion relation, $\mathrm{Re}(\bar{k}_{sc})$, versus $\mathrm{Re}(\bar{\Omega})$ as well as the power spectrum. In the pulse frame, $\bar{k}'_{sc}$ is complex and $\bar{\Omega}'$ is real. In the lab frame, $\bar{k}_{sc}$ is complex as is $\bar{\Omega}$; however, the imaginary portions of $\bar{k}_{sc}$ and $\bar{\Omega}$ are linked to one another via the relation

$$\mathrm{Im}(k)\,c \;=\; \mathrm{Im}(\Omega) \quad . \tag{29}$$

This relation arises from the fact that in steady state, all quantities are functions only of $x' = x - ct$, and not of $t' = t$.

In order to construct the dispersion relation and the power spectrum, we proceed as follows. We numerically solve the quartic dispersion relation as given by (26), which yields $\bar{k}'_{sc}(\bar{\Omega}')$. The change of variables $x' = x - ct$, $t' = t$, yields $\partial_x = \partial_{x'}$ and $\partial_t = \partial_{t'} - c\partial_{x'}$, or, when operating on a_{II},

$$k' \;=\; k \quad , \tag{30a}$$

$$\Omega' \;=\; \Omega - kc \quad . \tag{30b}$$

We seek the quantity $k_{II}(\Omega_{III})$, the strongly coupled wavenumber as a function of the frequency at a detector located in Region III, behind the pulse. When the relations (30) are utilized, we can determine $k_{II}(\Omega_{III})$ in terms of the steady state variables, namely,

$$\begin{aligned} k_{II}(\Omega_{III}) \;&=\; k'_{II}(\Omega'_{III} - k'_{III}c) \\ &= k'_{II}(\Omega'_{III} - \Omega'_{III}2) \end{aligned}$$

$$= k'_{II}(\Omega'_{III}/2)$$

$$= k'_{II}(\Omega'_{II}/2) \quad . \tag{31}$$

In going from line one to line two of (31) we have used the uncoupled dispersion relation, $k'_{III} = -\Omega'_{III}/(2c)$, and in going from line three to line four of (31) we have used the fact that $\Omega'_{III} = \Omega'_{II} = \Omega'_{I}$.

The reader may question why we have gone to such great lengths to derive the dispersion relation in the steady state variables $x' = x - ct$, $t' = t$, solve it, and then transform back to lab variables. In the $\{x', t'\}$ variables, Ω' is real and it is straightforward to solve for $k'(\Omega')$, where k' is complex. In terms of the lab variables, however, both Ω and k are complex, with the subsidiary condition $\mathrm{Im}(\Omega) = c[\mathrm{Im}(k)]$. In order to solve the dispersion relation in the lab frame, it must be split into its real and imaginary parts, where first, (29) is used to replace $\mathrm{Im}(\Omega)$ with $c\,[\mathrm{Im}(k)]$. The imaginary part of the dispersion relation then yields $\mathrm{Im}(k)$ as a function of $\mathrm{Re}(\Omega)$ and of $\mathrm{Re}(k)$, e.g., $\mathrm{Im}(k) = F[\mathrm{Re}(k),\ \mathrm{Re}(\Omega)]$. When $\mathrm{Im}(k) = F[\mathrm{Re}(k), \mathrm{Re}(\Omega)]$ is substituted back into the real part of the dispersion relation, there exists an expression for $\mathrm{Re}(k)$ in terms of $\mathrm{Re}(\Omega)$ which must then be solved. Such a procedure is much more tedious, and thus we have chosen to solve the dispersion relation in terms of the steady state variables $x' = x - ct$ and $t' = t$.

At a given spatial location inside the pulse the modes obey the coupled dispersion relation constrained by the late time condition, $\mathrm{Im}(\Omega) = [\mathrm{Im}(k)]c$. However, once the pulse has passed this location, the excited modes no longer interact. This transition from a region of interaction, where the instability is excited, to a region of no interaction, where the backscattered light is detected, causes a frequency shift. The frequency shift arises from the continuity of the Doppler shifted frequency across the coupling/no coupling interface (i.e., the pulse edge), namely

$$\Omega_{II} - k_{II}c = \Omega_{III} - k_{III}c \quad , \tag{32}$$

or

$$\Omega_{III} = \Omega_{II} - (k_{II} - k_{III}c)$$

$$= \frac{1}{2}(\Omega_{II} - k_{II}c) \quad , \tag{33}$$

since $k_{III}c = -\Omega_{III}$ is the uncoupled dispersion relation for the scattered light wave.

In Figs. 4 - 7 we plot the power spectrum as would be detected by a spectrometer behind the pulse and its associated wavenumber as functions of frequency for the cases of no coupling, weak coupling, strong coupling, and ultra-strong coupling, respectively. The reader should be aware that while the power spectrum is a physically measurable quantity, its associated wavenumber is not, but it is presented here as an exercise in understanding. In these figures we have chosen parameter values typical of short pulse experiments at Lawrence Livermore National Laboratory (LLNL) [16], $n/n_c = 0.01$, $T_e = 30$ eV, $\lambda_0 = 1.05$ μm, $Z = 2$, $A = 4$, and $L = .02$ cm.

Fig. 4 is a plot of the wavenumber, $\mathrm{Re}(\overline{k})$ versus $\mathrm{Re}(\overline{\Omega})$, as discussed above, where $\overline{k} \equiv k_{sc}/k_0$ and $\overline{\Omega} \equiv \Omega_{III}/\omega_a$. Curve a corresponds to the "forward" ion acoustic wave, curve b to the "backward" ion acoustic wave, and curve c to the backscattered light wave. The "forward" scattered light wave is several orders of magnitude off this scale and for the experimental parameters indicated never interacts with the other three waves, even as $v_0/c \to 1$.

We have labelled curves a, b, and c as "backward" or "forward" to identify the modes even though this figure indicates that the three modes of interest are all "backward", i.e., propagating in the direction opposite to the pulse group velocity. If the dispersion relation had been plotted in the limit of an infinite length interaction region, so that the pulse is at a fixed spatial location for all time, then these curves would have been the usual dispersion relations: namely, curve a would be $\Omega = kC_s$, or $\overline{k} = 2\overline{\Omega}$; curve b would be $\Omega + 2\omega_a = -kC_s$, or $\overline{k} = -2(\overline{\Omega} + 2)$; and curve c would be $\Omega = -kc$, or $\overline{k} = -2\epsilon\overline{\Omega}$.

Figs. 5 - 7 are plots of the power spectrum, $\exp\{2[\mathrm{Im}(\overline{k}_{II})\overline{L}]\}$, and its associated wavenumber, $\mathrm{Re}(\overline{k}_{II})$, as functions of $\mathrm{Re}(\overline{\Omega}_{III})$. In these figures, the pump strength is $v_0/c = 0.0005$, 0.01, and 0.3, or the laser intensity is $I = 1.24 \times 10^{12}$, 4.95×10^{14}, and 4.6×10^{17} W/cm^2 ($\overline{\gamma}_0 \equiv \gamma_0/\omega_a = 0.2$, 4.1, and 123), respectively. The power spectra, shown on a scale different than that of their associated wavenumbers, result from the existence of a region of unstable coupling between the scattered light wave and the "forward" ion acoustic

wave.

In Fig. 5(a) the power spectrum is symmetrically peaked about $\mathrm{Re}(\overline{\Omega}) = 0$, which corresponds to the resonant matching condition, as is anticipated for weak coupling. In Fig. 5(b), curves a and b are the wavenumbers of the ion acoustic waves, and curve c is that of the scattered light wave.

In Figs. 6 the unstable coupling region now extends over the range of frequencies $-20 \leq \mathrm{Re}(\overline{\Omega}) \leq 5$. The power spectrum peaks slightly to the left of $\mathrm{Re}(\overline{\Omega}) = 0$ and is no longer symmetric about the peak. It has a long, blue-shifted tail, but also extends to the red of the incident wave, which is located at $\mathrm{Re}(\overline{\Omega}) = -1$. Curves a and b are the wavenumbers of the ion acoustic waves, and curve c is that of the scattered light wave.

In the ultra-strong coupling case (Figs. 7), where $2\overline{\gamma}_0(C_s/c)^{1/2} > 1$, the power spectrum extends over a range of several hundred acoustic frequencies about the resonance matching point. Curve a corresponds to the power spectrum calculated behind the pulse. It has an even longer blue tail than when the instability is strongly coupled, and extends further to the red as well. For the sake of comparison we have included in this figure curve b, which is a plot of the power spectrum without taking into account the frequency shift induced by the transition from a region of strong coupling to region of no coupling. Mathematically, this corresponds to a plot of $\exp\{2\ \mathrm{Im}[\overline{k}_{II}(\overline{\Omega}_{II})]\ L\}$ versus $\mathrm{Re}(\overline{\Omega}_{II})$. Curves c and d are the wavenumbers of the ion acoustic waves, and curve e is that of the scattered light wave.

Curve b never extends to the blue, i.e., it is identically zero for frequencies $\mathrm{Re}(\overline{\Omega}_{II}) < -1$, where $\mathrm{Re}(\overline{\Omega}_{II}) = -1$ corresponds to the incident wave frequency. The evolution of curve b as the coupling strength increases is that for weak coupling it is symmetrically peaked about $\mathrm{Re}(\overline{\Omega}_{II}) = 0$ and extends over a range of frequencies $-4\sqrt{2}\overline{\gamma}_0 < \mathrm{Re}(\overline{\Omega}_{II}) < 4\sqrt{2}\overline{\gamma}_0$, where, for weak coupling, $\overline{\gamma}_0 < 1$. As v_0/c is increased, $\overline{\gamma}_0$ eventually exceeds unity. When strongly coupled or ultra-strongly coupled (as in Fig. 6 or 7), the power spectrum peaks at $\mathrm{Re}(\overline{\Omega}_{II}) = \overline{\gamma}_0^{2/3}/2 - 1$, and extends over the range of frequencies $-1 < \mathrm{Re}(\overline{\Omega}_{II}) < (2\overline{\gamma}_0^2)^{1/3}$, e.g., the power spectrum never extends to the blue of the incident wave frequency, $\mathrm{Re}(\overline{\Omega}_{II}) = -1$ ($\omega = \omega_0$).

There are startling similarities between the predicted power spectrum of SBBS and that of SRBS (stimulated Raman backscatter), as is evident by comparing Fig. 7a to Fig. 1b of Ref. [16]. For both instabilities, when the frequency shift caused by the coupling/no coupling transition the modes undergo at the back edge of the pulse is neglected, the power spectrum never extends to the blue of the pump wave. However, when the frequency shift is taken into account the power spectrum acquires a blue shifted tail but extends to the red as well. These similarities arise from the physics of the short pulse (continuity in the Doppler shifted frequency across the back edge of the pulse) independent of the instability mechanism inside the pulse.

Experimentally, then, we would predict that the backscattered light collected at a detector behind the pulse would peak in frequency near the resonant frequency. The spectrum should extend to the red of the pump wave, and, provided that sensitivity is not an issue, there should be a blue-shifted tail.

IV. NUMERICAL ANALYSIS

In the lab frame, the complete set of equations (1) may also be written as [8]

$$\left[\frac{\partial}{\partial t} - V_g \frac{\partial}{\partial x}\right] a_1 = \gamma_0 (a_+ - a_-) \quad , \tag{34a}$$

$$\left[\frac{\partial}{\partial t} - C_s \frac{\partial}{\partial x}\right] a_+ = \gamma_0 a_1 \quad , \tag{34b}$$

$$\left[\frac{\partial}{\partial t} - C_s \frac{\partial}{\partial x} - 2i\omega_s\right] a_- = \gamma_0 a_1 \quad , \tag{34c}$$

where $a_+ - a_- \equiv a_2$. Here we have dropped the ∂_x^2 term compared to the ∂_x term operating on a_1 in (34a) and the ∂_x term compared to unity operating on a_1 in (34b) and (34c), as is appropriate in both the weakly coupled and the strongly coupled limits. This representation is useful when performing a numerical analysis because each equation in (34) contains a convective differential operator, and a coupling term of order $\gamma_0 \Delta t$; thus, only one algorithm is necessary when solving the above set of equations. We use the algorithm outlined by Van Leer et al. [20] to convect the waves, whereas the wave coupling is handled using a first-order

accurate scheme which requires $\gamma_0 \Delta t \ll 1$. We have found such a scheme to be tractable in previous numerical work on SBBS [8].

In terms of the steady state variables, where $x' = x - ct$, and $t' = t$, the set equations (34) is of the form

$$\left[\frac{\partial}{\partial t'} - 2c\frac{\partial}{\partial x'}\right] a_1 = \gamma_0(a_+ - a_-) \quad , \tag{35a}$$

$$\left[\frac{\partial}{\partial t'} - c\frac{\partial}{\partial x'}\right] a_+ = \gamma_0 a_1 \quad , \tag{35b}$$

$$\left[\frac{\partial}{\partial t'} - c\frac{\partial}{\partial x'} - 2i\omega_a\right] a_- = \gamma_0 a_1 \quad . \tag{35c}$$

In this set of equations we have approximated $c = C_s \approx c$.

We have solved (35) in both the weakly coupled and the strongly coupled limits. In the $\{ a_1, a_+, a_- \}$ representation the weakly coupled limit is tantamount to legislating $a_- = 0$, which requires the growth rate to be small compared to ω_a so that the a_- mode, which is shifted from the a_+ mode by $2\omega_a$ in the frequency domain, lies outside the bandwidth of the a_+ mode and is therefore not excited. In the strongly coupled limit, where the growth rate is of the order of or greater than the ion acoustic frequency, it is necessary to solve the complete set of equations (35).

Fig. 8 is a plot in the pulse frame of the magnitude of the backscattered light wave versus position inside the pulse at 21 different time intervals ranging from $\omega_a t = 0$ to $\omega_a t = 60$, with $\Delta t = 3/\omega_a$ and $\bar{\gamma}_0 = 0.4$. The instability grows from the initial condition $a_1(x', t') = 1$, where here, x' denotes the position inside the pulse ($0 < x' < L$). The wave amplitude increases with time for a time $t = L/c$ (two light wave transit times across the pulse) after which time there in no more temporal growth and thus the instability temporally saturates, leaving a spatial gain across the pulse.

The instability in the strong coupling limit responds similarly. The differences are that when strongly coupled, the wave amplitudes are being driven more strongly and therefore grow to greater magnitude: furthermore, they grow at a different rate [$\Gamma \sim (2\gamma_0^2\omega_a)^{1/3}$ as opposed to $\Gamma \sim \gamma_0$ when weakly coupled]; and finally, the spatial gain across the pulse is

$\kappa = \gamma_0/(\sqrt{2}c)$ when weakly coupled as opposed to $\kappa \sim (\gamma_0^2\omega_a)^{1/3}/c$ when strongly coupled.

Fig. 9 depicts the numerical and analytical temporal growth rates as a function of time in both the weak and strong coupling limits. Curve a is the numerical weak coupling result, which, along its flat-top, is overlaid by the analytic weak coupling result, denoted as curve b. For the weak coupling case, $\gamma_0 = 0.4$. Curve b should overlay curve a for times less than a light wave transit time across the pulse, or for times $t \leq L/(2c)$ $(\bar{t} \equiv \omega_a t \leq \epsilon\bar{L} = 30$, where $\epsilon = 0.5$ and $\bar{L} \equiv k_0 L)$. As predicted, the growth rate falls to zero between one light wave transit time $(\bar{t} = 30)$ and two light wave transit times $(\bar{t} = 60)$.

Curve c is the numerical strong coupling result, which, for times less than a light wave transit time across the pulse $(\bar{t} < 30)$ should be approximated by the analytic strong coupling result, curve d. For curves c and d, $\bar{\gamma}_0 = 2.0$. For times $\bar{t} \leq 35$, there is a 2% discrepancy between the analytic approximation and the numerical result. This discrepancy stems from the size of $\bar{\gamma}_0$, i.e., if $\bar{\gamma}_0$ had been larger, or if we had retained more terms in the series expansion of the growth rate as given by (24), there would have been even better agreement between curves c and d.

We have also examined the spatial growth rates as a function of position inside the pulse in both the weak and strong coupling limits, as shown in Fig. 10. Curve a is the numerical weak coupling result, which is obtained by plotting $|a_1(\bar{x}')|$ at a time long compared to two light wave transit times across the pulse. Curve b is the analytic result $\kappa \equiv \gamma_0/(\sqrt{2}c)$, with $\gamma_0 = 0.4$. Curve a corroborates the analytic result, curve b.

Curve c is the numerical strong coupling result which was obtained in the same manner as in the weak coupling limit, only with $\bar{\gamma}_0 = 2.0$. Curve d is the analytic result $\kappa = (\omega_a/c)\left|\exp[-i\pi/3]\bar{\gamma}_0^{2/3} - (2/3) + (4/9)\exp[i\pi/3]\bar{\gamma}_0^{-2/3} + (16/81)\bar{\gamma}_0^{-4/3} + ...\right|$. There is roughly a 4% difference between the analysis and the numerics, a deviation which could be minimized by either increasing the coupling strength $\bar{\gamma}_0$ or by retaining more terms in the series expansion of κ.

V. SUMMARY

We have derived an exact solution to the weakly coupled ($\gamma_0 < \omega_a$) short pulse SBBS instability and approximate analytic solutions to the strongly coupled ($\gamma_0 > \omega_a$) short pulse SBBS instability. In either case, the instability rapidly enters a steady state where there is a spatial gain in wave amplitude between the front and the back of the pulse.

Since there is temporal growth for an amount of time much less than the signal collection time, the power spectrum is dominated by the steady state, i.e., it is independent of the chosen set of initial conditions. The steady state response is not affected by whether the instability grows from a legislated set of initial conditions (as has been done in this work) or if it were seeded by thermal fluctuations (as in Ref. [9]).

We have found that the physics of the short pulse as well as that of the Brillouin instability itself has an affect on the backscattered power spectrum. First, the backscattered light wave amplifies as it traverses the laser pulse, with a spatial amplification rate $\mathrm{Im}[k(\Omega)]$ that can be calculated from the strongly coupled mode equations describing Brillouin scattering together with the steady state condition $\mathrm{Im}(\Omega) = [\mathrm{Im}(k)]c$. The range of frequencies over which a growing mode is excited is then stretched when the backscattered light wave crosses the back edge of the pulse and enters a region where it is no longer coupled to plasma density fluctuations. This transition from a region of coupling (c) to a region of no coupling (uc) maintains continuity of the Doppler shifted frequency, $\Omega_c - k_c c = \Omega_{uc} - k_{uc} c$, resulting in a shift of the detected frequency from the frequency at which the mode was amplified, i.e., $\Omega_{uc} = \Omega_c - (k_c - k_{uc})c$.

When the modes are weakly coupled the unstable region of the dispersion relation gives rise to a power spectrum which is symmetrically peaked about the resonant matching frequency, $\mathrm{Re}(\overline{\Omega}) = 0$, and is red-shifted from the pump, located at $\mathrm{Re}(\overline{\Omega}) = -1$. As the coupling strength increases, the peak of the power spectrum slightly shifts from $\mathrm{Re}(\overline{\Omega}) = 0$, and it acquires a blue-shifted tail, but extends to the red as well. When the power spectrum is plotted without taking into account the frequency shift caused by the short pulse (i.e.,

by the fact that the excited modes decouple as they exit the back side of the pulse) we find that it cannot extend to the blue side of the incident pump frequency, as was found for short pulse SRBS in Ref. [16].

We have also solved the weakly and strongly coupled short pulse SBBS problems numerically, and find good agreement with our analytic results. The numerics validate the analytic temporal growth rates and spatial gain rates. The numerical analysis also shows the absence of temporal growth after two light wave transit times across the plasma.

For the sake of simplicity, we have neglected the effects of damping. If ion acoustic wave damping (ν) had been included, the temporal growth rate of the instability would have been $\Gamma = [\gamma_0^2 + (\nu/2)^2]^{1/2} - \nu/2$ in the weak coupling limit. When the instability is strongly coupled, the growth rate $\Gamma \sim (2\gamma_0^2\omega_a)^{1/3} > \omega_a \gg \nu$, and damping has a negligible effect. Incorporation of damping also modifies the spatial gain of the steady state in a similar manner, but is negligible when $\gamma_0 \gg \nu$.

We have also neglected nonlinear effects. When strongly or ultra-strongly coupled, there can be significant depletion of the front part of the pulse by the instability, and this will act to limit the reflectivity. Pulse shape may affect the instability as well. As a pulse traverses a particular spatial location inside plasma, the instability will ramp up to the strongly coupled limit through a regime where it is weakly coupled. As the back side of the pulse reaches the spatial location of interest, the intensity is falls and the instability will go through another regime where it is weakly coupled.

For the ultra-strong coupling parameters used here (which were chosen similar to those of the short pulse experiments conducted at LLNL) the value of $\omega/(k\bar{v}_e)$ is still small compared to unity [$\omega \sim 0.5(2\gamma_0^2\omega_a)^{1/3}$], thereby justifying the fluid treatment in this paper. However, for much higher intensities (roughly a hundred times greater) kinetic effects and relativistic effects will become important. It is interesting to note, however, that in the regime $\omega/(k\bar{v}_e) \gg 1$, where the wave phase velocity is much greater than the electron thermal velocity, the analysis performed here still would still apply. In this regime the ponderomotive pressure dominates the electron thermal pressure. Thus, taking the limit $T_e \to 0$ of Eqs. (1)

is appropriate when $\omega/(k\bar{v}_e) \gg 1$.

For some ultra-strong coupling parameters (such as those used in this study) the set of equations (1) should be modified to include the effects of space-charge separation. The set of equations (1) is derived by imposing quasi-neutrality, which is valid provided $\omega \ll \omega_{pi}$. When the instability is in the ultra-strong coupling limit ω can exceed ω_{pi} since $\mathrm{Im}(\omega) \sim (2\gamma_0^2\omega_s)^{1/3}$ even in the steady state. In this case Eq. (1b) should be modified to include the operator $1 + \omega_{pi}^{-2}\partial_t^2$ operating on the ponderomotive potential. [In the limit $\omega \ll \omega_{pi}$, this factor just reduces to unity, as it should when weakly or even strongly coupled.] We anticipate that the inclusion of the $\omega_{pi}^{-2}\partial_t^2$ term operating on the ponderomotive potential will act to decrease the magnitude of the power spectrum as well as the range of frequencies which generate the power spectrum.

ACKNOWLEDGMENTS

We would like to thank Dr. W. B. Mori for many illuminating discussions.

This work was performed under the auspices of the U.S. Department of Energy by the Lawrence Livermore National Laboratory under Contract No. W-7405-ENG-48.

REFERENCES

[1] V. P. Silin, Sov. Phys. JETP **21**, 1127 (1965).

[2] J. F. Drake, P. K. Kaw, Y. C. Lee, G. Schmidt, C. S. Liu, and M. N. Rosenbluth, Phys. Fluids **17**, 778 (9174).

[3] D. W. Forslund, J. M. Kindel, and E. M. Lindman, Phys. Fluids **18**, 1002 (1975).

[4] K. Nishikawa and C. S. Liu, in *Advances in Plasma Physics*, Vol. 6, edited by A. Simon and W. B. Thompson, (Wiley and Sons, New York, 1976).

[5] W. L. Kruer, *The Physics of Laser Plasma Interactions*, (Addison-Wesley, Reading, MA, 1988).

[6] D. L. Bobroff and H. A. Haus, J. Appl. Phys. **38**, 390 (1967).

[7] E. A. Williams and R. R. McGowan, in *Inertial Confinement Fusion*, edited by K. A. Brueckner, (American Institute of Physics, New York, 1992), p. 325.

[8] D. E. Hinkel, E. A. Williams and R. L. Berger, forthcoming in Physics of Plasmas, September, 1994.

[9] Ph. Mounaix, D. Pesme, W. Rozmus, and M. Casanova, Phys. Fluids B **5**, 3304 (1993).

[10] H. A. Baldis, D. M. Villeneuve, B. La Fontaine, G. D. Enright, C. Labaune, S. Baton, Ph. Mounaix, D. Pesme, M. Casanova, and W. Rozmus, Physics Fluids B **5**, 3319 (1993).

[11] M. D. Perry and G. Mourou, Science **264**, 917 (1994).

[12] D. C. Eder, P. Amendt, L. B. DaSilva, R. A. London, B. J. MacGowan, D. L. Matthews, B. M. Penetrante, M. D. Rosen, S. C. Wilks, T. D. Donnelly, R. W. Falcone, and G. L. Strobel, Phys. Plasmas **1**, 1744 (1994).

[13] W. B. Mori, C. D. Decker and W. P. Leemans, IEEE Trans. on Plasma Sci. **21**, 110 (1993).

[14] S. C. Wilks, W. L. Kruer and W. B. Mori, IEEE Trans. on Plasma Sci. **21**, 120 (1993).

[15] Wm. M. Wood, C. W. Siders, and M. C. Downer, IEEE Trans. on Plasma Sci. **21**, 20 (1993).

[16] C. B. Darrow, C. Coverdale, and M. D. Perry, Phys. Rev. Lett. **69**, 442 (1992).

[17] W. B. Mori, C. D. Decker, D. E. Hinkel, and T. Katsouleas, Phys. Rev. Lett. **72**, 1482 (1994).

[18] C. L. Tang, J. Appl. Phys. **37**, 2945 (1966).

[19] In this derivation we have utilized the expansion $\cosh(z\cos t) = \sum_{k=-\infty}^{k=+\infty} I_{2k}(z)\cos(2kt)$.

[20] B. Van Leer, J. Computational Phys. **23**, 276 (1977).

FIGURES

FIG. 1. Schematic of the short-pulse SBBS problem in the pulse frame of reference. The scattered light wave of Region I is amplified as it propagates through the pulse (Region II). Continuity of wave amplitude and phase is maintained as the light wave leaves the pulse and enters Region III.

FIG. 2. A space-time diagram of the causal regions of influence. At point a, in the early time regime, the solution is determined by the initial conditions, but has yet to be influenced by the boundary conditions. At point b, in the late time regime, the solution is determined by the boundary condition at $x' = L$. At point c, in the intermediate time regime, the solution is influenced by both the initial and boundary conditions. For a spatially independent initial condition and a temporally independent boundary condition the early time solution is independent of space and the late time solution is independent of time.

FIG. 3. A schematic of the steady state short pulse problem in the pulse frame of reference. A scattered light wave in Region I is amplified as it travels through the pulse (Region II). As the wave exits the back side of the pulse, and enters Region III it leaves the interaction region and enters the regioe of detection. and continuity of wave amplitude and phase is maintained across the back side of the pulse.

FIG. 4. The uncoupled wavenumber, $\mathrm{Re}(\bar{k})$, where $\bar{k} \equiv k_{II}/k_0$, as a function of $\mathrm{Re}(\overline{\Omega})$, where $\overline{\Omega} \equiv \Omega_{III}/\omega_a$. Here, $n/n_c = 0.01$, $T_e = 30$ eV, $v_0/c = 0$, $\lambda_0 = 1.05$ μm, $Z = 2$, $A = 4$, $L = .02$ cm, and $\bar{\gamma}_0 = 0$. Curves a and b are the uncoupled ion acoustic waves. Curve c is the uncoupled scattered light wave. $\mathrm{Re}(\overline{\Omega}) = -1$ corresponds to the incident light frequency.

FIG. 5. (a) The weakly coupled power spectrum, $\exp\{2[\mathrm{Im}(\bar{k})\bar{L}]\}$, and (b) its associated wavenumber, $\mathrm{Re}(\bar{k})$, where $\bar{k} \equiv k_{II}/k_0$, as a function of $\mathrm{Re}(\bar{\Omega})$, where $\bar{\Omega} \equiv \Omega_{III}/\omega_a$. Here, $n/n_c = 0.01$, $T_e = 30$ eV, $v_0/c = 0.0005$, $I = 1.24 \times 10^{12}$ W/cm^2, $\lambda_0 = 1.05$ μm, $Z = 2$, $A = 4$, $L = .02$ cm, and $\bar{\gamma}_0 = 0.2$. Curves a and b are the ion acoustic waves. Curve c is the scattered light wave. $\mathrm{Re}(\bar{\Omega}) = -1$ corresponds to the incident light frequency. The power spectrum and the dispersion relation are detected behind the pulse.

FIG. 6. (a) The strongly coupled power spectrum, $\exp\{2[\mathrm{Im}(\bar{k})\bar{L}]\}$, and (b) its associated power spectrum, $\mathrm{Re}(\bar{k})$, where $\bar{k} \equiv k_{II}/k_0$, as a function of $\mathrm{Re}(\bar{\Omega})$, where $\bar{\Omega} \equiv \Omega_{III}/\omega_a$. Here, $n/n_c = 0.01$, $T_e = 30$ eV, $v_0/c = 0.01$, $I = 4.95 \times 10^{14}$W/cm^2, $\lambda_0 = 1.05$ μm, $Z = 2$, $A = 4$, $L = .02$ cm, and $\bar{\gamma}_0 = 4.1$. Curves a and b are the ion acoustic waves. Curve c is the scattered light wave. $\mathrm{Re}(\bar{\Omega}) = -1$ corresponds to the incident light frequency. The power spectrum and the dispersion relation are detected behind the pulse.

FIG. 7. (a) The ultra-strongly coupled power spectrum, $\exp\{2[\mathrm{Im}(\bar{k})\bar{L}]\}$, and (b) its associated wavenumber, $\mathrm{Re}(\bar{k})$, where $\bar{k} \equiv k_{II}/k_0$, as a function of $\mathrm{Re}(\bar{\Omega})$, where $\bar{\Omega} \equiv \Omega_{III}/\omega_a$. Here, $n/n_c = 0.01$, $T_e = 30$ eV, $v_0/c = 0.3$, $I = 4.6 \times 10^{17}$W/cm^2, $\lambda_0 = 1.05$ μm, $Z = 2$, $A = 4$, $L = .02$ cm, and $\bar{\gamma}_0 \sim 123$. Curve a is the power spectrum calculated by including the frequency shift induced by crossing the back edge of the pulse, across which the Doppler shifted frequency is constant. Curve b is the power spectrum calculated negelecting this induced frequency shift. Curves c and d are the dispersion curves for the ion acoustic waves. Curve e is the dispersion curve for the scattered light wave. $\mathrm{Re}(\bar{\Omega}) = -1$ corresponds to the incident light frequency.

FIG. 8. The magnitude of the backscattered light wave in the weak coupling limit as a function of position inside the pulse at time intervals $\Delta t = 3/\omega_a$, ranging from time $t = 0$ to time $t = 60/\omega_a$. The wave grows temporally for two light wave transit times, and then enters a steady state where there is a spatial gain across the pulse.

FIG. 9. The temporal growth rate as a function of time. In the weak coupling limit, ($\gamma_0 = 0.4$), curve a, which is the weakly coupled numerical result, agrees with curve b, the approximate analytic growth rate of the early time regime, $\Gamma \sim \gamma_0$. In the strong coupling limit ($\gamma_0 = 2.0$), curve c, which is the strongly coupled numerical result agrees to within 2 % with the approximate analytic growth rate of the early time regime, $\Gamma \sim (2\gamma_0^2\omega_a)^{1/3}$, curve d, before the instability enters a steady state.

FIG. 10. The spatial gain across the pulse as a function of position inside the pulse. In the weak coupling limit, ($\gamma_0 = 0.4$), curve a, which is the weakly coupled numerical result agrees with curve b, the approximate analytic spatial gain, $\kappa \sim \gamma_0/(2^{1/2}c)$, except near the pulse boundaries where the fact that the spatial gain is not quite exponential is significant. In the strong coupling limit ($\gamma_0 = 2.0$), curve c, which is the strongly coupled numerical result, agrees to within 4 % with the approximate analytic spatial gain, $\kappa \sim (\gamma_0^2\omega_a)^{1/3}/c$, curve d, except near the pulse boundaries.

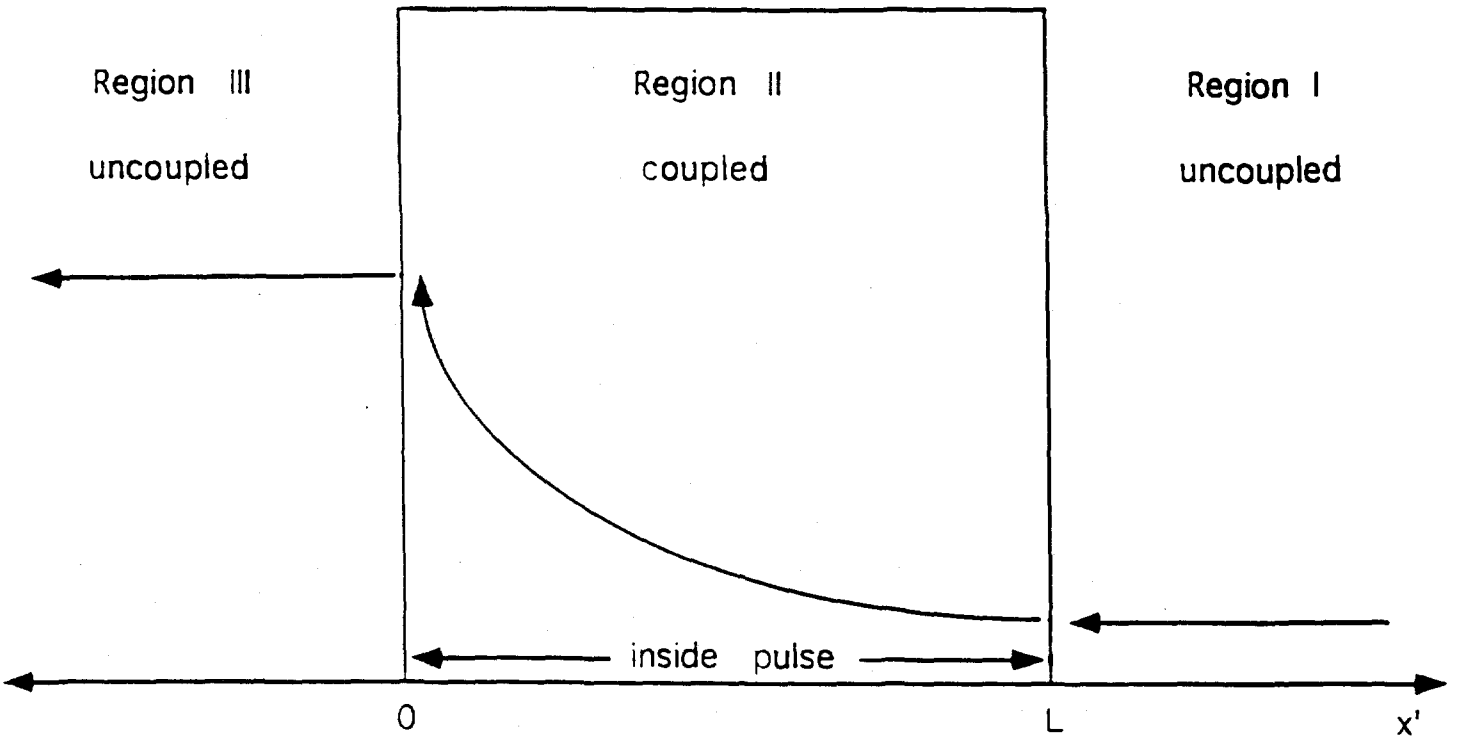
Region III
uncoupled
Region II
coupled
Region I
uncoupled
inside pulse
0
L
x'

Fig. 1

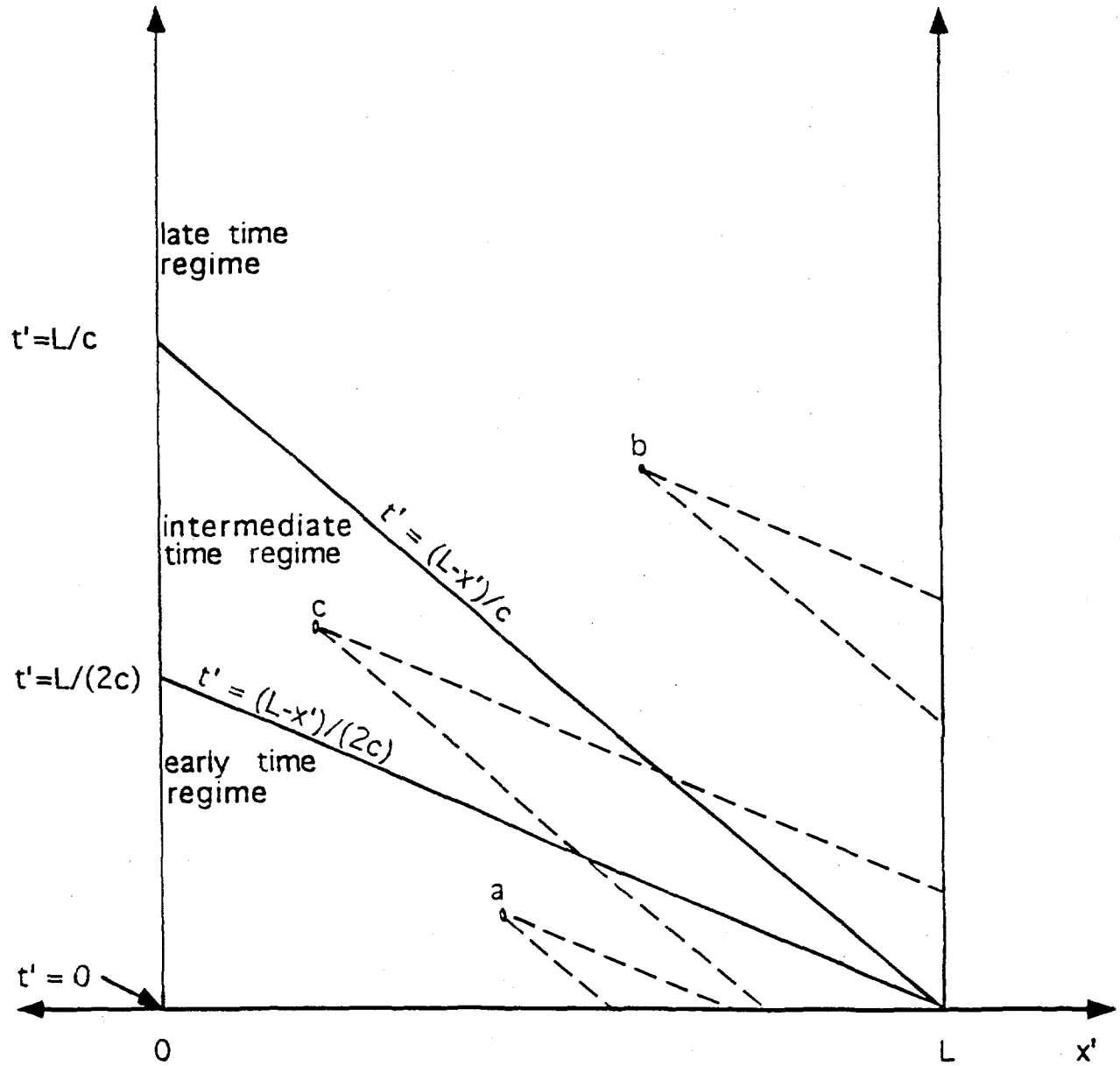
late time
regime
t'=L/c
b
intermediate
time regime
t' = (L-x')/c
c
t'=L/(2c)
t' = (L-x')/(2c)
early time
regime
a
t' = 0
0
L
x'

Fig. 2

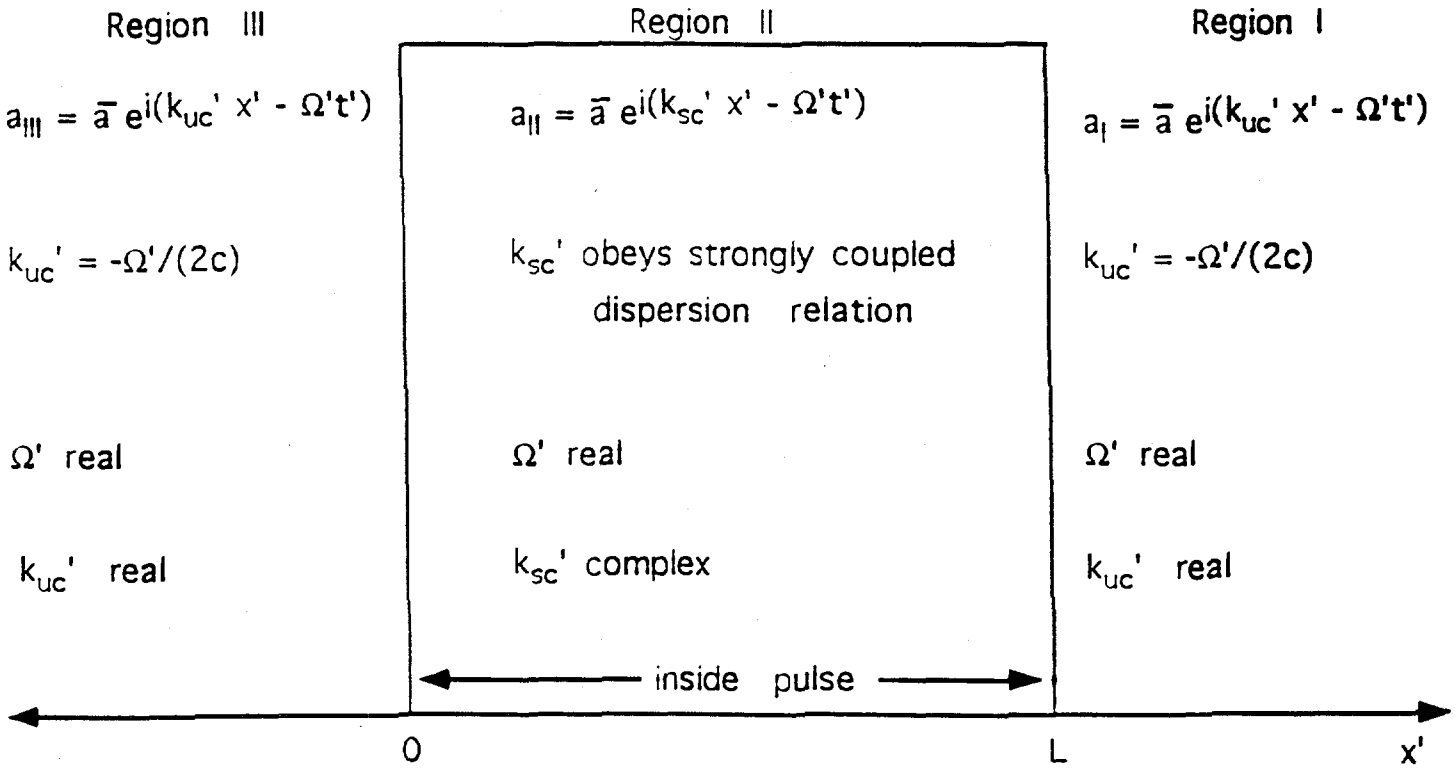
Region III
Region II
Region I
$a_{III} = \bar{a}\, e^{i(k_{uc}' x' - \Omega' t')}$
$a_{II} = \bar{a}\, e^{i(k_{sc}' x' - \Omega' t')}$
$a_{I} = \bar{a}\, e^{i(k_{uc}' x' - \Omega' t')}$
$k_{uc}' = -\Omega'/(2c)$
k_{sc}' obeys strongly coupled dispersion relation
$k_{uc}' = -\Omega'/(2c)$
Ω' real
Ω' real
Ω' real
k_{uc}' real
k_{sc}' complex
k_{uc}' real
inside pulse
0
L
x'

Fig. 3

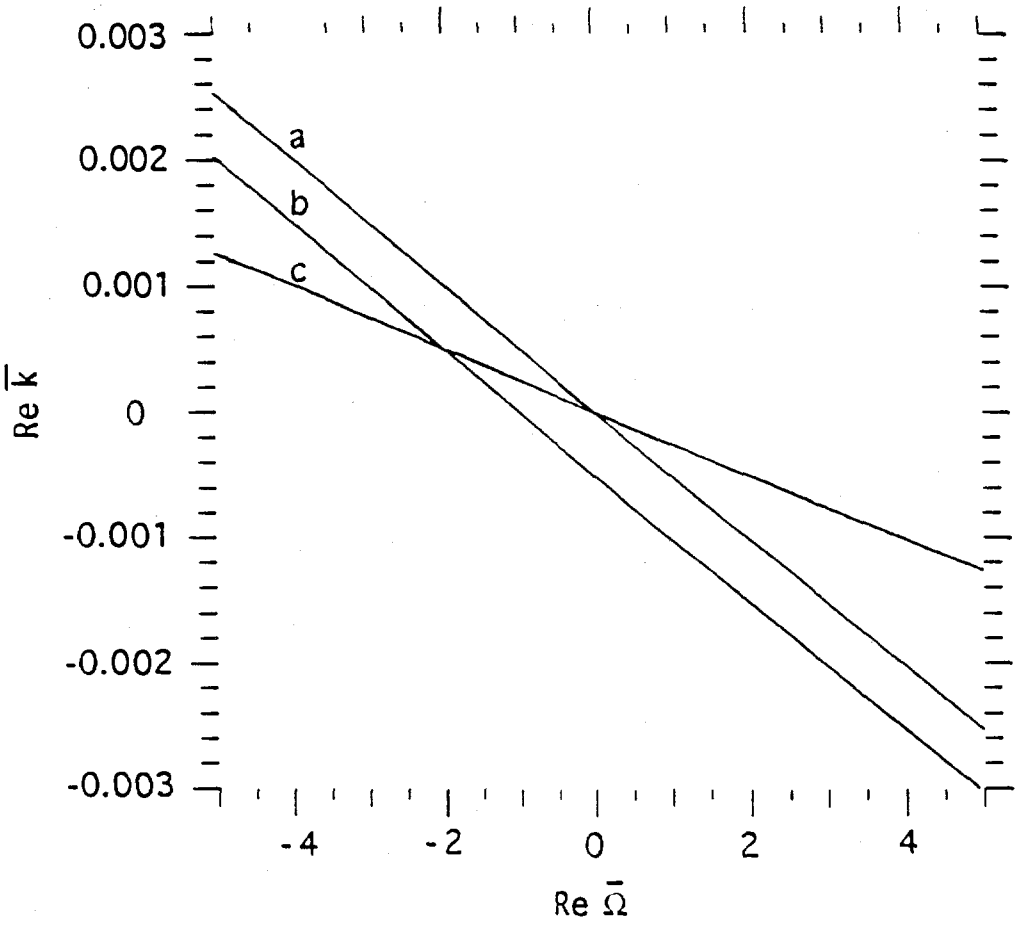

Fig. 4

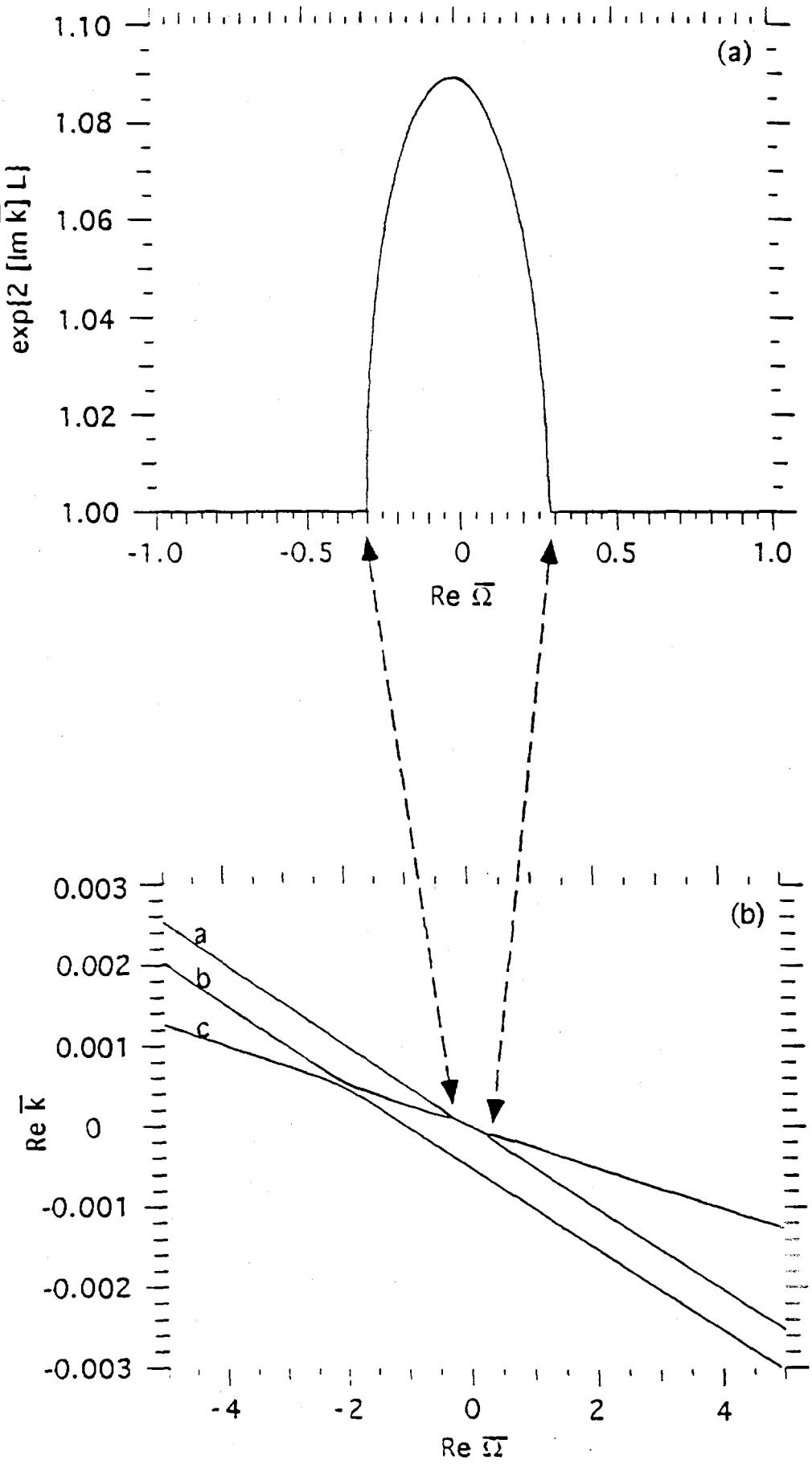
(a)
1.10
1.08
1.06
1.04
1.02
1.00
exp{2 [Im k̄] L̄}
-1.0
-0.5
0
0.5
1.0
Re Ω̄
(b)
0.003
0.002
0.001
0
-0.001
-0.002
-0.003
Re k̄
a
b
c
-4
-2
0
2
4
Re Ω̄

Fig. 5

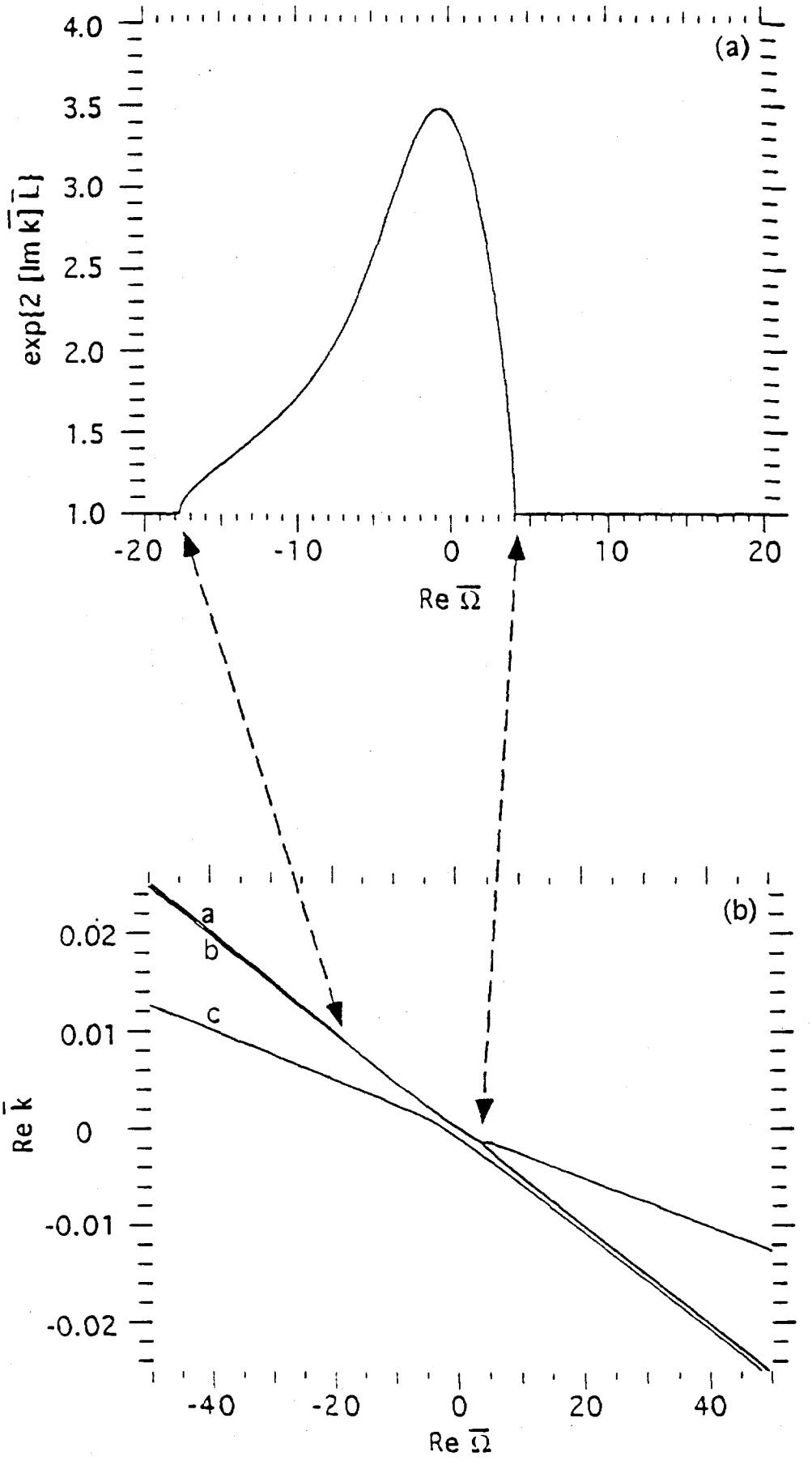
(a)
4.0
3.5
3.0
2.5
2.0
1.5
1.0
exp{2 [Im k̄] L̄}
-20
-10
0
10
20
Re Ω̄
(b)
a
b
c
0.02
0.01
0
-0.01
-0.02
Re k̄
-40
-20
0
20
40
Re Ω̄

Fig. 6

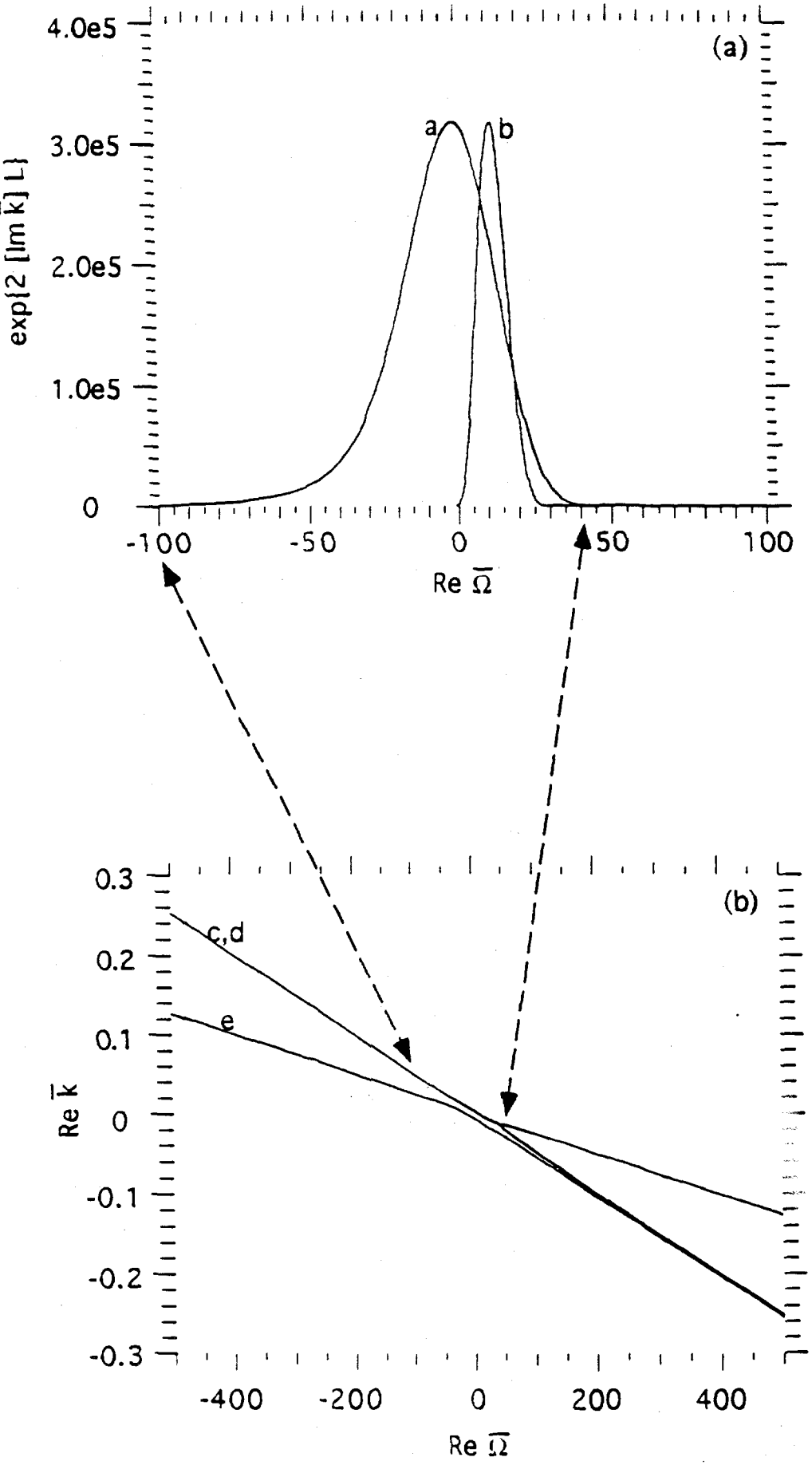
(a)
4.0e5
3.0e5
2.0e5
1.0e5
0
exp{2 [Im k̄] L̄}
a
b
-100
-50
0
50
100
Re Ω̄
(b)
0.3
0.2
0.1
0
-0.1
-0.2
-0.3
Re k̄
c,d
e
-400
-200
0
200
400
Re Ω̄

Fig. 7

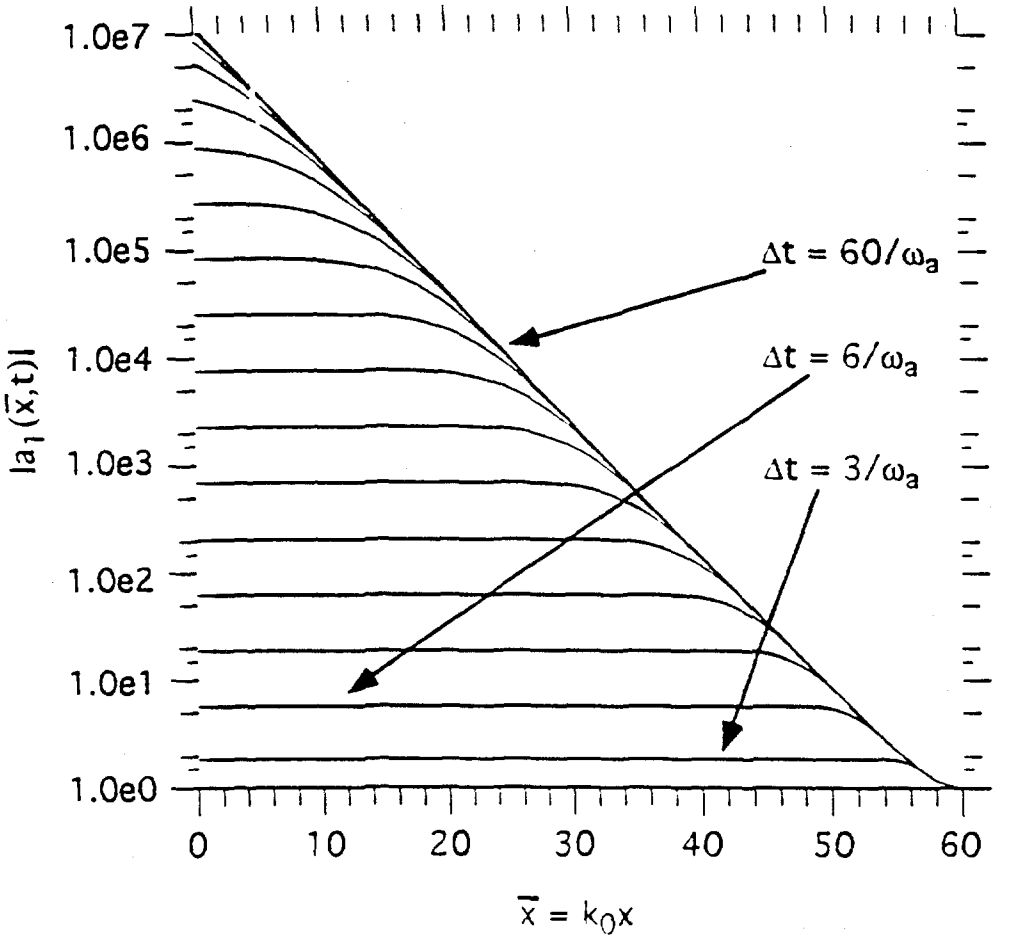
1.0e7
1.0e6
1.0e5
1.0e4
1.0e3
1.0e2
1.0e1
1.0e0
$|a_1(\bar{x},\bar{t})|$
$\Delta t = 60/\omega_a$
$\Delta t = 6/\omega_a$
$\Delta t = 3/\omega_a$
0
10
20
30
40
50
60
$\bar{x} = k_0 x$

Fig. 8

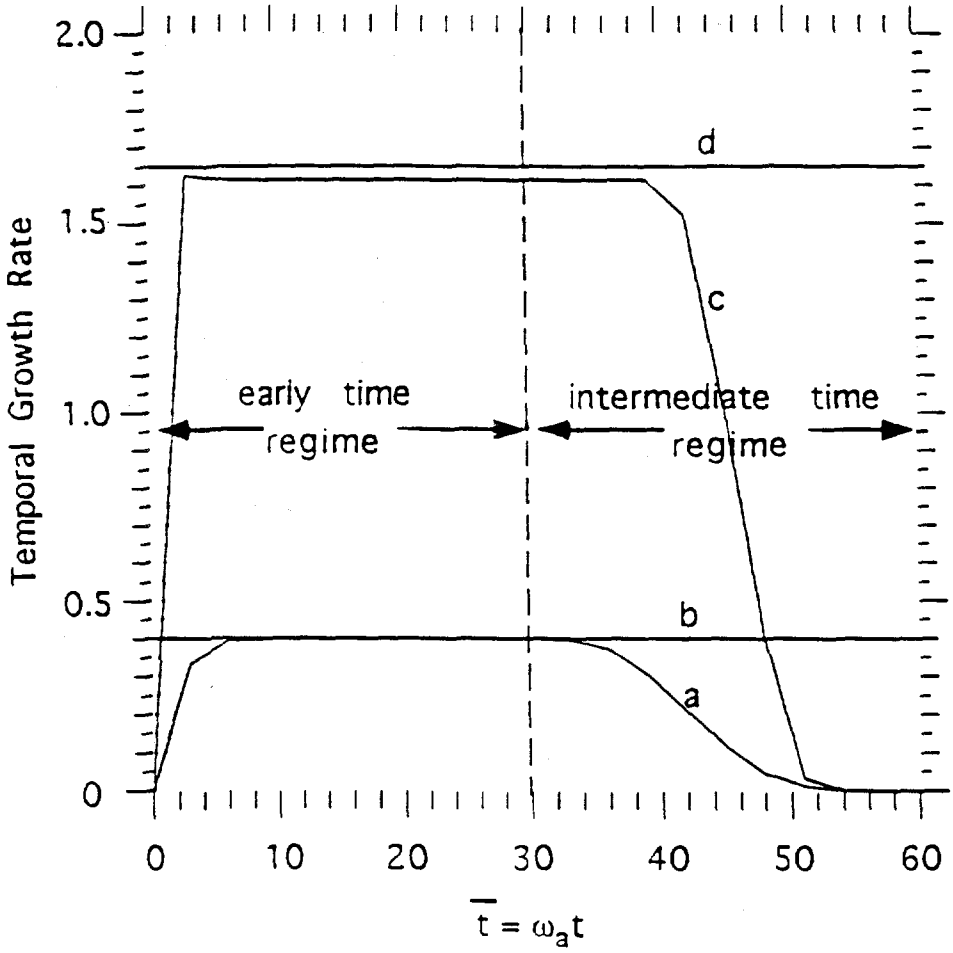
2.0
1.5
1.0
0.5
0
Temporal Growth Rate
d
c
b
a
early time regime
intermediate time regime
0
10
20
30
40
50
60
$\bar{t} = \omega_a t$

Fig. 9

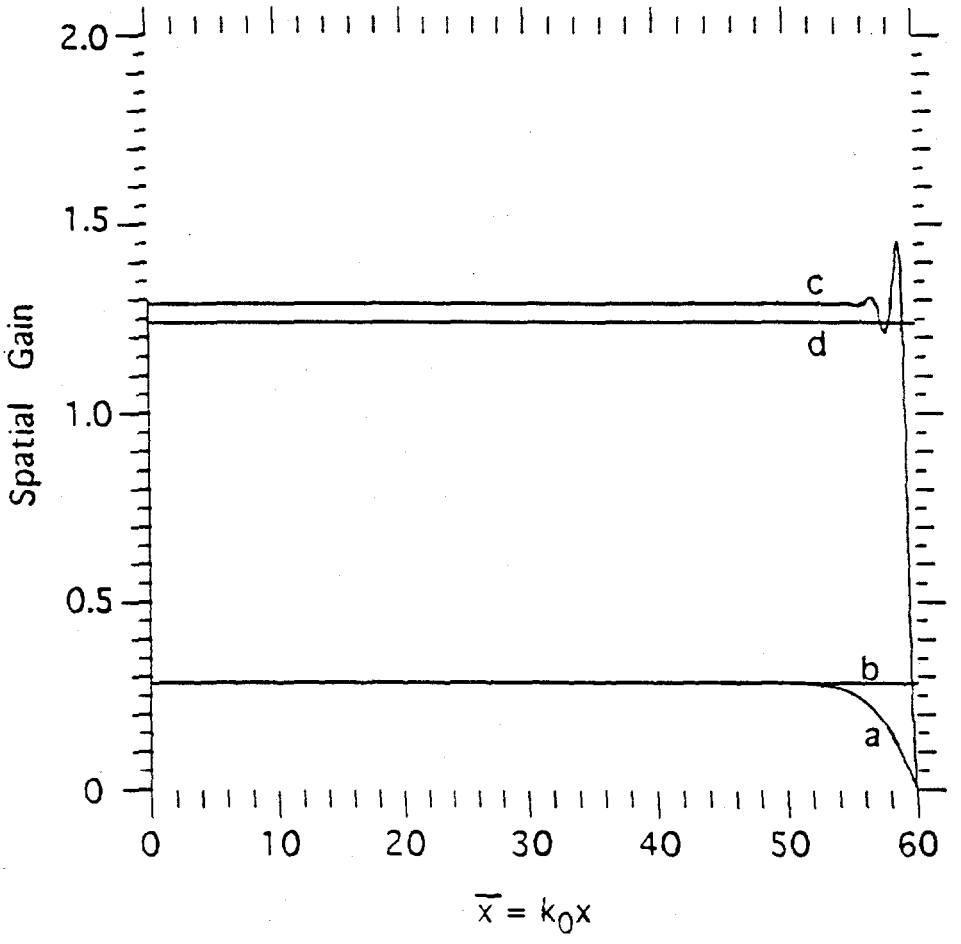

Fig. 10